# STUDY ON KNUDSEN FLOW THROUGH MEMBRANE PORES USING ANALYTICAL APPROXIMATION AND MONTE CARLO METHOD

A THESIS SUBMITTED TO THE GRADUATE DIVISION OF THE
UNIVERSITY OF HAWAI‘I IN PARTIAL FULFILLMENT
OF THE REQUIREMENTS FOR THE DEGREE OF

MASTER OF SCIENCE

IN

CIVIL ENGINEERING

DECEMBER 2011

By
Yong Shi

Thesis Committee:

Albert S. Kim, Chairperson
Michelle H. Teng
Tao Yan
Yi Zuo

We certify that we have read this thesis and that, in our opinion, it is satisfactory in scope and quality as a thesis for the degree of Master of Science in Civil Engineering.

THESIS COMMITTEE

_____
Chairperson

_____

_____

_____

# Acknowledgments

I hereby express my deep and sincere gratitude to my advisor, Dr. Albert S. Kim, for his encouragement, guidance, and willingness to always set me on the right path during the undertaking of my graduate research. I am honored and privileged to have worked under his guidance. I also extend my thanks to Dr. Michelle H. Teng, Dr. Tao Yan and Dr. Yi Zuo for agreeing to be on my thesis committee. Thank you for their efforts in reviewing my thesis and for providing valuable comments.

I would like to thank the Maui High Performance Computing Center (MHPCC) for providing the High Performance Computing (HPC) resources. I also thank the American working class and the Government for allowing forergners like myself to pursue higher education in their esteemed institutions.

I extend my thanks to members of the Computational Environmental Physics Laboratory: Rong Yuan, Ying Guo and Om Das, for the stimulating discussions I have had with them on various topics that include mathematics, computer programming, econophysics and econometrics, etc. Furthermore, I acknowledge the constant encouragement received over the years from my friends: Ying, Ming and Xiaoyan.

Last, but not the least, I thank my parents for their never ending encouragement, love, and support throughout my life. Thank you for always being there and for being so understanding. This thanks also extends to my sisters, Wen and Xiaoyan.

# Abstract

In this study, Knudsen diffusion of low-pressure gases of infinite mean free path through various tubes is studied using the integral equation theory, standard diffusion theory, and Monte Carlo simulations. We investigated the transmission probabilities (TPs) of linearly diverging-converging, sinusoidally bulging, and periodic tubes as compared with TPs of conventional straight cylinders. An exact analytic solution for the TP through the straight cylindrical tube was developed using the standard diffusion theory with a linear concentration approximation. Integral equation theories for the TPs through the diverging-converging and bulging tubes were developed. Monte Carlo simulation techniques were applied to calculate TPs through all the tube types whose azimuthal symmetry was held with tube radius changing only along the axial coordinate (z). The equivalent radii of these tubes are calculated as root-mean-squares of the z-dependent radius to have the same internal void volume. The linearly diverging-converging and sinusoidally bulging tubes provide noticeably higher TPs than those of the equivalent straight tubes. Periodic tubes show that if the tube length scaled by the equivalent diameter is on the order of or greater than the periodicity coefficient (equal to the number of peaks on the tube wall), the TP of the periodic tube is larger than that of the equivalent straight tube. In general, an opening at the tube inlet significantly enhances the Knudsen diffusion.

# Contents

# List of Figures

# Nomenclature

| | |
|---|---|
| $\bar{v}$ | Mean molecular speed |
| $\epsilon$ | Peak amplitude of tube, i.e., a dimensionless distance from the imaginary tube surface of radius $r_0$ at the mid-point (at $z = L/2$) to the peak of the diverging-converging or bulging tube |
| $\eta_{\mathrm{dir}}^{C}$ | Direct TP of Clausing's analytic solution, taken from Walsh's work |
| $\eta_{\mathrm{dir}}^{SKL,\mathrm{MC}}$ | Direct TP calculated using Monte Carlo simulations in this study |
| $\eta_{\mathrm{ind}}^{SKL,\mathrm{MC}}$ | Indirect TP calculated using Monte Carlo simulations in this study |
| $\eta_{\mathrm{tot}}^{SKL}$ | Total TP as a summation of direct TP by Clausing's integral equation theory and indirect TP by our theory developed in this study |
| $\eta_{\mathrm{dir}}^{PP}$ | Direct TP of Pollard & Present's theory for the first order correction |
| $\eta_{\mathrm{dir}}^{W,\mathrm{Asym}}$ | Direct TP of Walsh's asymptotic form |
| $\eta_{\mathrm{ind}}^{C,\mathrm{Asym}}$ | Indirect TP of Clausing's asymptotic form |
| $\eta_{\mathrm{ind}}^{K}$ | Indirect TP corresponding to the original Knudsen diffusivity, $D_K$ |
| $\eta_{\mathrm{ind}}^{PP}$ | Indirect TP of Pollard & Present's theory for the first order correction |
| $\eta_{\mathrm{ind}}^{SKL}$ | Indirect TP analytically derived in this study |
| $\eta_{\mathrm{tot}}^{PP}$ | Total TP of Pollard & Present's theory for the first order correction |
| $\lambda$ | Mean free length of molecules |

$\phi$ Angle at the inlet and outlet of the diverging-converging tute in magnitude

$a$ Radius of a straight cylindrical tube

$d$ Diameter of a straight cylindrical tube

$d_{\mathrm{eq}}^{\mathrm{bulging}}$ Equivalent diameter of this bulging tube

$d_{\mathrm{eq}}$ Equivalent diameter of a tube of an axially varying diameter having the identical void volume and lenth of a straight tube

$d_{\mathrm{eq}}^{\mathrm{div-conv}}$ Equivalent diameter of the conically diverging-converging tube of Equation 4.2.2

$D_K$ Knudsen diffusivity for a semi-infinitely long tube of diameter $d$

$d_p(z)$ Diameter of a tube as a function of the axial position $z$ in the cylindrical coordinate

$L$ Length of a tube

$L'$ Half length of a tube

$L_{\mathrm{cross}}/d_{\mathrm{eq}}$ Dimensionless crossing distance at which the TPs of periodic and straight tubes are identical

$M$ Molecular weight

$n(z)$ Number concentration of molecules in the tube as a function of axial coordinate $z$

$n_1$ Number concentration of molecules at the tube inlet

$n_2$ Number concentration of molecules at the tube outlet

$N_w$ Number of molecules passing through the central cross-sectional area per unit time

$r(z)_{\mathrm{bulging}}$ Radius of the bulging (sinusodially diverging-converging) tube as a function of $z$

$r(z)_{\mathrm{div-conv}}$ Radius of the conically diverging-converging tube as a function of $z$

| | |
|---|---|
| $r'$ | Distance of molecules, traveling without collisions |
| $r_0$ | Inlet and outlet radius of diverging-converting and bulging tubes |
| $r_1(z)$ | Radius at the left side of the diverging-converting and bulging as a function of $z$ |
| $r_2(z)$ | Radius at the right side of the diverging-converting and bulging as a function of $z$ |
| $T$ | Temperature |
| $V$ | Volume of void spaces in a tube |
| $z$ | Axial coordinate of a tube |

# Chapter 1

# Introduction

Knudsen diffusion (KD) phenomena of gases through narrow pores was discovered more than a century ago [12, 13], but still remains as a partially unsolved problem due to chemical, physical, and geometrical complexities of porous media. For a low-pressure gas passing through a long tube, the mean free path of the gas molecules can be much larger than the pore dimensions. The majority of traveling gas molecules collide with the internal tube wall. Inter-molecular collisions rarely occur in this low concentration system and therefore the normal Brownian diffusion does not play a significant role in the gas diffusion. If a constant pressure gradient exists along the tube by maintaining fixed concentrations at the inlet and outlet, KD is the dominant gas transport mechanism and can be effectively used for separation of binary or mixed gases in various engineering applications such as isotope separation [28], hydrogen extraction [14], and membrane distillation [3, 7].

The first experimental study for free-molecular gas flow through straight tubes (i.e., a geometrically confined space) was performed by Knudsen in 1909 [12]. In his work, Knudsen gave an approximate expression to estimate the number of molecules passing a given cross-section of the tube per unit time, which has been proved to be valid in his experiment when the observed flow approaches to a limiting value near zero pressure, i.e. low molecular concentration. Clausing [4, 5] used the classical kinetic theory and developed mathematical formulation of such free-molecular flow problems. Later investigators re-derived Clausing's equation by different techniques and also formulated the problem for other geometries. Iczkowski et al. [9], reformulated the integral equation for conical

tubes, and Richley and Reynolds [22] developed the integral equations for converging and diverging rectangular slots.

In Clausing's approach, the general expression for the wall flux distribution is an integral equation, and hence an analytic solution in closed form is fundamentally formidable. The remaining flow characteristics can be, however, readily calculated once the wall flux distribution is determined. An assumption has been made for the straight tube problem by Pollard and Present [19] where molecular concentration linearly varies along the straight tube. They thus developed an analytical approximation of the diffusion coefficient under the condition of a long tube with small diameter, which may be regarded as the first order correction of Knudsen's approximate expression.

Instead of numerically solving the Clausing integral equation and directly calculating the TP by Knudsen's or Pollard and Present's approximation, the Monte Carlo method is an alternative method to simulate the diffusive transport. Talley and Whitaker [27] reported that both the Monte Carlo simulation and Clausing theory give us identical results for straight tubes within statistical uncertainties, and recently, Lobo et al [17] also made a comparison between these two approaches for the TPs of conical tubes. While the integral equation theory is limited to simple geometries such as straight and diverge/converge slots/tubes, Monte Carlo methods are available for almost arbitrary geometries.

The KD coefficient, i.e., the proportionality between diffusive gas flux and the concentration gradient, has the asymptotic form of $D_K = \bar{v}d/3$ for a long tube of length $L\,(\gg d)$, where $\bar{v}$ is the mean molecular speed following Maxwell distribution and $d$ is the (cylindrical) pore diameter. After Knudsen's original work, researchers investigated effects of various pore structures and physico-chemical interactions between molecules and pore walls on the KD using theoretical and simulation approaches. In addition, although Knudsen diffusivity may be evaluated with high accuracy for straight tubes by the Clausing theory or Monte Carlo simulation method, both of them would encounter the same difficulty that computer programming is required or, even if codes are available, computation is often expensive if a long tube is investigated.

To the best of our knowledge, it is generally accepted that a shorter tube has a higher KD coefficient and any structural variations from the straight, round cylindrical tube hampers the KD-limited gas transport except for diverging tubes or slots at the inlet (see

next section for detailed review). Although KD has been widely used to explain gaseous transport in engineering processes using porous media, effects of pore structures on the KD were seldom studied in detail. In this study, we first try to developed an analytic solution of the TP for a cylindrical tube by employing Pollard and Present's assumption of the linear concentration profile along the tube length and the results will be testified by Clausing's integral equation theory and Monte Carlo simulations as well. Later, the same method will be applied for a diverging-converging tube as well. Second, as far as we know, the study of the integral equation theory for the diverging-converging and sinusoidally bulging tubes has not been reported. This study will developed the integral equation theory on these two kinds of tubes and the result will also be compared with that of Monte Carlo simulations. Finally, we also investigated the TP for the periodic tubes and the effect of the internal structures on the TP by using Monte Carlo simulations

# Chapter 2

# Review of Literatures

## 2.1 Knudsen's Approximate Expression

In Knudsen's early work [12], an approximate expression to estimate the number of molecules passing through a given cross-section of the tube per unit time was given by

$$N = -\frac{16a^3}{3m\bar{v}}\frac{\mathrm{d}p}{\mathrm{d}z} \tag{2.1.1}$$

where $a$ is the tube radius, $m$ is the molecular mass, $\bar{v}$ is the mean molecular speed, and $\mathrm{d}p/\mathrm{d}z$ is the pressure gradient along the tube length. The experimental studies [12] showed that the observed diffusive flow approaches to a limiting value of Eq.(2.1.1) when molecular concentration is low. We define $J$ as the number of passing molecules per cross-sectional area of the straight tube in unit time so that $J = N/\pi a^2$, which is represented as

$$J = -D_k\frac{\mathrm{d}n}{\mathrm{d}z} \tag{2.1.2}$$

where $D_k$ is the Knudsen diffusion coefficient and $\mathrm{d}n/\mathrm{d}z$ is the gradient of the molecular concentration along the tube length. The transmission probability (TP) $\eta$ is defined as a fraction of molecules entered the (left) inlet of a tube, exited at the (right) outlet, without returning to the (left) reservoir and formulated as

$$\eta = \frac{N_{\mathrm{out}}}{N_{\mathrm{in}}} = \frac{J_{\mathrm{out}}}{J_{\mathrm{in}}} \tag{2.1.3}$$

The relationship between the diffusion coefficient $D_k$ and the transmission probability $\eta$ for the Knudsen flow is

$$\eta = \frac{D_k}{\bar{v}L/4} = \frac{N/\pi a^2}{\frac{1}{4}\bar{v}L(-\mathrm{d}n/\mathrm{d}z)} \tag{2.1.4}$$

Using $p = nkT = \pi nm\bar{v}^2/8$ together with Eq.(2.1.1), Knudsen's transmission probability for a long straight tube is expressed as

$$\eta = \frac{4d}{3L} \tag{2.1.5}$$

## 2.2 Clausing's Integral Equation Theory

Clausing [4, 5] formulated rigorous mathematical representations of the TP and independently dealt with direct and indirect TPs. The direct TP ($\eta_{\mathrm{dir}}$) is a fraction of incoming molecules that pass through the tube without any collision with the tube wall so that this is dominant when the tube length is of the same order as the tube diameter. Walsh developed a light radiation theory to determine the illumination at any point on a disc by a second coaxial disc, the radiation from which, in any direction, is proportional to the cosines of the angle between that direction and the normal to the surface and calculated a fraction of the whole radiation flux from the first disc which falls on the second disc [29]. The two coaxial discs of the same diameter, facing each other in parallel, are geometrically equivalent to the inlet and outlet cross-sections of the straight cylindrical tube. Clausing adopted Walsh's solution as the direct TP and developed the self-consistent integral equation theory (IET) to calculate the indirect TP ($\eta_{\mathrm{ind}}$), i.e., the fraction of molecules entering the inlet exit with at least one collision with the tube wall. The IET intrinsically dealt with the conditional probability that, given a molecule colliding with the tube wall at a location $0 < z < L$, the next random flight of the molecule from the collision point leads to the molecule's escape at the tube outlet. All prior collisions and the last collision with the tube wall were implicitly counted in the integral equation. Clausing's exact numerical solution of the indirect TP was later verified using Monte Carlo simulations [27].

Clausing, however, failed to give the asymptotic limit of Knudsen's indirect TP, $\eta_{\rm ind}^{K} = 4d/3L$ (an equivalent dimensionless form of $D_K$) for a long cylindrical tube ($L \gg d$), but gave only the half the original expression, i.e., $\eta_{\rm ind}^{C,\,\rm Asym} = 2d/3L$. The direct TP for a long tube seems to be negligible as it converges to $\eta_{\rm dir}^{W,\,\rm Asym} = d^2/4L^2$ (which we derived from Walsh's analytic solution). However, we found that the direct TP plays an important role when the indirect TP is corrected using higher order terms of $d/L$. (See next sections.)

## 2.3 Pollard and Present's Approximation

Pollard & Present (PP) [19] derived an analytic approximation of KD for self-diffusing molecules in a pure gas at a uniform pressure gradient in a long capillary tube. As shown in Figure 4.1, the planar symmetry was set up at the center of the tube ($z = 0$), and the tube inlet and outlet are located at $z = -L/2$ and $+L/2$, respectively. Two fractions of molecules that enter the central cross-section (at $z = 0$) after the last collision with the tube wall and a neighboring molecule were individually calculated and superimposed afterward. Various cases of length scales of the tube diameter $d\,(= 2a)$, tube length $L$, and the molecular mean free path $\lambda$ were investigated using the Boltzmann factor, $e^{-r'/\lambda}$, assigned as a probability that a molecule of the mean free path $\lambda$ travels a distance $r'$ after the last collision. PP's theory reached the proper asymptotic limit of the total TP (as a sum of direct and indirect TPs) for an infinite $\lambda$ and provided the first order correction as $\eta_{\rm tot}^{PP} = \frac{3d}{4L}\left(1 - \frac{4d}{3L}\right)$. In general, the mean free path is inversely proportional to the gas pressure or (equivalently) concentration. Effects of the linear concentration on the KD coefficient through $\lambda$ was studied later by Flory and Cutler [8].

It is worthwhile analytically to compare Clausing's and PP's theoretical approaches as we found that they are partially contradictory to each other. Clausing's integral equation theory dealt with all the possible collision events (at least one with the tube wall) of exiting molecules in the past and provided an accurate numerical solution of the indirect TP through a tube of an arbitrary length, but failed to reach the asymptotic limit of the indirect TP for a long tube. On the other hand, PP's theoretical framework was based on the symmetric axial coordinate $z$ running from $-L'$ to $+L'$ where $L'\,(= L/2)$ is the half-length. Instead of adopting Walsh's exact solution, PP calculated the direct TP at the tube

center ($z = 0$) as a function of $\lambda$ using the same mathematical setup for calculating indirect TP shown in Figure 4.1. Because PP did not individually derive direct and indirect TPs, but only total TP, we followed PP's theory and separately recalculated the indirect TP as $\eta_{\text{ind}}^{PP} = \frac{4d}{3L}\left(1 - \frac{3d}{2L}\right)$ for an infinite $\lambda$ and the direct TP as the difference between the total and indirect TPs as $\eta_{\text{dir}}^{PP} = d^2/L^2$. Note that, interestingly, $\eta_{\text{dir}}^{PP}$ is the fourfold asymptotic limit of Walsh's exact solution, $\eta_{\text{dir}}^{W,\,\text{Asym}}$ (as discussed above). Mistakenly, PP's direct TP deals with only a half-cylinder with length $L'(= L/2)$, which suggests a correction of PP's direct TP by replacing $L$ of $\eta_{\text{dir}}^{PP}$ with $2L'$. This discrepancy can be easily understood by Walsh's setup of the two facing discs of equal size at distance $L$. PP calculated "net" flux through a circular cross-section at the tube center $(z = 0)$ from two half tubes of length $L/2$ at (left) inlet and (right) outlet sides. As a summary, PP failed to reproduce Walsh's solution of asymptotic direct TP for an infinite $\lambda$, but succeeded to produce indirect TP for a long tube with a first order correction. For approximate solutions of KD with an infinite $\lambda$, it must be reasonable to take Walsh's exact solution for the direct TP (as it is) and use PP's axial coordinate centered at $z = 0$, where $-L/2 < z < L/2$, to calculate appropriate analytic solutions for the indirect TP.

## 2.4 Other Theoretical Models

A dusty gas model was developed for gaseous diffusion through porous media under conditions of uniform [10] and linear[11] pressure profiles. Bosangquet's relationship was re-confirmed using uniform pressure, i.e., the inverse of effective diffusivity is the sum of inverses of normal and Knudsen diffusivities at a low gas pressure. Porous media was composed of stationary giant molecules, called dusty particles. Pore spaces were assumed to be much smaller than the dimensions of the porous media, which are characterized using macroscopic parameters of porosity and tortuosity without specific description of microscopic pore structures. For a constant (non-zero) pressure gradient, the net molecular flux of binary species was calculated by assuming a linear concentration across the porous media. In both papers [10, 11], Evans III et al. emphasized the molecular flux of binary gas species, assuming that the normal diffusivity is dependent on the gas concentration; and implied that the KD coefficient is independent of internal structures of porous media given

porosity and tortuosity. Further development of the dusty gas model included effects of pressure and temperature gradient on KD phenomena [18]. Present and DeBethune investigated separation of a binary gas mixture through a long tube at low pressure[20]. In the Knudsen regime, the separation factor reaches a maximum, i.e., the square root of the mass ratio and similar to the dusty gas model, the viscous effects were treated as a small additive perturbation on the gas flow.

While studies described above are limited to straight cylindrical tubes or uniform porous media, Iczkowski et al. applied Clausing's theory to diverging and converging conical orifices and found moderately good agreement with experimental observations [9]. In-depth studies of KD phenomena through diverging and converging tubes and slots can be found in technical reports of National Aeronautics and Space Administration[24, 22, 23].

Recent research focused on the microscopic aspects of pore compositions and structures and their chemical and physical influences on KD. Bhatia and Nicholson examined the tortuosity for diffusion of light gases in nanoporous carbons using the Oscillator model of low pressure transport which incorporated van der Waals attraction. They indicated that the direct use of the KD model to meso- or nano-scale pores is misleading due inconsistencies arising from neglect of van der Waals forces [1]. The Oscillator model[2] was specifically applied to methane transport in carbon slit pores by Lim and Bhatia [16]. Krishna and van Baten [15] used molecular dynamics (MD) simulations to investigate the concentration dependence of Fick diffusivities for methane, ethane, propane, n-butane, n-pentane, n-hexane, n-heptane, and cyclohexane in cylindrical silica mesopores; and indicated that zero-loading diffusivity is consistently lower than the classical KD formula due to molecular adsorption on the pore surfaces. On the other hand, Ruthven et al. [25] discussed the validity of the KD model by analyzing experimental permeance data for several light gases (He, Ar, $N_2$, $CH_4$, $C_3H_8$) in a mesoporous silica membrane; and indicated that the experimental diffusivities are proportional to $\sqrt{T/M}$ in conformity with the Knudsen model, where $T$ is the temperature and $M$ is the molecular weight. From the KD research discussed above, it seems to be adequate that the KD model is applied to micro- and meso-scale pores without significant molecular adsorption on pore walls; and molecular adsorption due to van der Waals interaction noticeably reduces the KD coefficient. Although these studies provided in-depth understanding of the KD at the molecular

scale phenomena (molecular adsorption, surface diffusion, microscopic roughness of pore surfaces, and collision elasticity), pore geometries were all assumed to be straight cylinders or rectangular slots. Investigation of the KD phenomena influenced by pore geometry (especially periodicity) is in a burgeoning stage. Here, we restrict our theory and simulations to the KD phenomena, including micro- or meso-pores of various geometry with negligible adsorption.

## 2.5 Monte Carlo Simulation

To the best of our knowledge, Davis' work was the first simulation study using the Monte Carlo method to investigate effects of tube/pore structures on the TP [6]. Pipe structures tested include a straight cylindrical tube, a cylindrical elbow, an annulus of two concentric cylinders, a straight cylindrical tube with restricted openings, and a straight cylindrical tube with restricted openings and a central blocking plate. All of the simulation results showed that the transmission probabilities are smaller than that of the straight cylindrical tube of the same length, calculated using the integral equation theory.

Talley and Whitaker later conducted Monte Carlo simulations to study Knudsen flow in porous media. Simulations of molecular transport in the Knudsen regime through the straight round cylindrical tube of an arbitrary length validated analytic approximations for those through sufficiently short and long cylindrical tubes [27]. The Knudsen flow through a converging-diverging tube (having a similar shape to a hourglass) has been studied and the results indicated that "significant reductions in the flow rate can occur for channels having the same average diameter but varying degrees of curvature in the direction of flow". A representative tube dimension was chosen as the average radius along the hourglass-like converging-diverging tube. In our opinion, however, the root-mean-square of the varying radius along the tube channel can provide a more meaningful representation of the equivalent (constant) radius so that the equivalent straight tube has an equal internal volume to that of the converging-diverging tube or other types. (See next section for mathematical details.)

Overall, effects of pore structures on KD were studied using computer simulations. Due to mathematical complexity, analytic solutions are very limited to a simple

geometry such as a straight cylindrical tube (with little variations) for limiting cases only. A plethora of simulation studies so far concluded that any structural modification from the conventional cylinder noticeably reduces the TP per given length and void volume. A comprehensive review of Knudsen's original work and research activities in the past century can be found elsewhere [26].

# Chapter 3

# Related Approaches

As discussed in the preceding sections, this study will investigate three basic approaches, i.e., approximation analysis, integral equation theory and Monte Carlo simulation, to evaluate the TP and compare them with each other for various geometries.

## 3.1 Approximate Analysis

After a thorough review of the prior studies described above, we found that Clausing's approximation of the linear escape probability, equivalent to Pollard & Present's assumption of the linear concentration, fails to hold the Galilean invariance and provides inaccurate coefficients of first- and higher-order terms of the total TP. Because the exact solution of the aperture contribution ($\eta_{\mathrm{dir}}^{\mathrm{C}}$) is available, we focused on developing an analytical solution of the indirect TP contributed by the tube wall. In this study, we applied the method developed by Pollard & Present [19] to the cylindrical and diverging-converging tubes and obtained the novel analytical solutions in closure form for each case. The approximate analysis will be described in details in the next section.

## 3.2 Integral Equation Theory

Although the integral equation theory to calculate the TP of a straight tube was reported by Clausing [4, 5] early back in 1932, this method applied for a non-straight tube such as diverging-converging and bulging tubes, as far as we know, has not been reported. For this reason, this section will briefly introduce the integral equation theory for

a cylindrical tube following Clausing's original work [5]. Later this method will be used to determine the TP for non-straight tubes, i.e. diverging-converging and bulging tubes.

As discussed above, the total TP can be summarized as

$$\begin{aligned} \eta_{\text{tot}} &= \eta_{\text{dir}} + \eta_{\text{ind}} \\ &= \omega_{ss}(L) + \int_0^L \omega_{sr}(z) w(z) \mathrm{d}z \end{aligned} \tag{3.2.1}$$

where $w(z)$ is the escape probability defined as

$$w\left(z\right) = \omega_{rs}\left(L - z\right) + \int_0^L \omega_{rr}\left(y - z\right) w\left(y\right) \mathrm{d}y \tag{3.2.2}$$

Here, we used the following definitions as extended from Clausing's work:

1. $\omega_{rr}\left(y\right)$ is the probability that a molecule, which in accordance with the cosine law, leaves a ring within an infinitesimal area $2\pi r\left(z\right) \mathrm{d}z$ at $z$, strikes directly onanother ring $2\pi r\left(z + y\right) \mathrm{d}z$ located at a distance $y$ from the first ring;

2. $\omega_{rs}\left(y\right)$ is the probability that a molecule leaving a ring $2\pi r\left(z\right) \mathrm{d}z$ at $z$ passes directly through a cross-section at the distance $y\left(= L - z\right)$;

3. $\omega_{sr}\left(z\right)$ is the probability averaged over the inlet cross-section $\pi r_0^2$ that a molecule leaving the section strikes directly on a ring $2\pi r\left(z\right) \mathrm{d}z$ at a distance $z$; and

4. $\omega_{ss}\left(z\right)$ is the probability, averaged over the inlet cross-section $\pi r_0^2$ that a molecule entering the tube directly passes the outlet cross-section at the distance $z\left(= L\right)$, which is identical to Eq. (4.1.1), i.e., Walsh's analytic solution that Clausing adopted.

Based on the definition, each probability can be derived in terms of the cosine law. See Appendix A for the derivation in details.

## 3.3 Monte Carlo Simulation

In this study, Monte Carlo simulations not only testify the results of simple geometries obtained by the integral equation theory and analytical approximation but also

provide the solution for almost arbitrary geometries. Here we adopted the method reported by Talley and Whitaker [27] to calculate the TP. The Monte Carlo algorithm employs the following procedures. (Appendix C shows the simulated procedures in details.)

1. A molecule is randomly positioned at the inlet circular cross-section at $z = -L/2$ and its flight direction toward the tube interior is arbitrarily chosen.

2. If the molecule leaves the tube at $z = +L/2$ immediately after it passes the inlet, the number of the escape event increases by one; if the molecule collides with the tube wall at a point inside the tube $(-L/2 < z < +L/2)$ on the wall $(r = d/2)$, the next flight direction is randomly selected from the last collision point.

3. (a) If the next flight leads the molecule to return to the (left) reservoir, then it is canceled; if the next flight guides the molecule to escape from the tube at the (right) outlet, then the number of the escape event is increased by one. In both cases, the simulation procedure goes to Step 1 with a new molecule created at the tube inlet. (b) If the molecule reaches a new point on the tube wall, a random collision will decide a new arbitrary direction, and a series of molecule-wall collisions continue until the flying molecule escapes at the tube outlet or returns to the (left) reservoir.

4. The number of molecule escaping from the tube divided by the total number of entering molecules provides the total TP, and a fraction of escaped molecules not colliding with the tube wall contributes to the direct TP. The difference between total and direct TP is the indirect TP.

# Chapter 4

# Results and Discussion

In this study, we investigated geometrical effects of radius-varying tubes on the KD coefficient in terms of the TP $(\eta)$ for an infinite $\lambda$. All the tubes have the same length $L$ and internal void volume $V$. For example, the conventional cylindrical tube has a constant diameter along the tube length; and others such as diverging-converging, bulging, and periodic tubes have diameters varying along the tube axis. The equivalent diameter $d_{\mathrm{eq}}$ was calculated based on the internal volume per unit length:

$$d_{\mathrm{eq}}^2 = \frac{4}{\pi}\frac{V}{L} = \frac{1}{L}\int_{-\frac{1}{2}L}^{+\frac{1}{2}L} d_p^2(z)\mathrm{d}z \tag{4.0.1}$$

where $d_p\,(z)$ is the tube diameter as a function of the axial position $z$ in cylindrical coordinates. The equivalent diameter of the straight (conventional) cylinder is equal to its diameter, i.e., $d_{\mathrm{eq}} = d$. We only consider variation of diameters along the tube axis so that azimuthal symmetry still remains valid for all the cases to be discussed; and tube interiors are transparent along the straight epi-center from inlet to outlet.

## 4.1 Cylindrical Tube

We revisit here the original theories of Walsh [29], Clausing [4, 5] and Pollard & Present [19], take mathematical advantages from each theory, and derive a novel analytic solution for the indirect TP assuming that the concentration profile is linear along the cylindrical tube axis. In addition, we individually calculate the direct and indirect TPs using Monte Carlo simulations following Talley and Whitaker's algorithm [27], and compare

systematically total TP (as a sum of direct and indirect TPs) with other results in the literature. Methods used in this section will be extended to tubes of various structures in later sections.

Clausing's solution for the direct TP (taken from Walsh's work [29]) can be explicitly represented as

$$\eta_{\mathrm{dir}}^{C} = \frac{\sqrt{L^2 + d^2} - L}{\sqrt{L^2 + d^2} + L} \tag{4.1.1}$$

For a sufficiently short tube ($L \ll d$), Eq. (4.1.1) converges to $1 - 2L/d$, indicating that the direct TP linearly decreases with respect to the dimensionless tube length; and for a very long tube ($L \gg d$), it reaches $d^2/4L^2$, which decreases much faster than the indirect TP of an order of $O(d/L)$.

Now, we develop an analytic solution of the indirect TP following PP's mathematical framework with the following assumptions: (1) the molecular flow is in steady state; (2) the flow is purely molecular, i.e., there are only hard collisions between molecules and the tube wall (i.e., inter-molecular collisions are negligible); and (3) the molecule collisions with the tube wall are taken as if gas molecules are diffusively reflected so that their velocity directions follow the cosine law without undergoing adsorption on the wall surfaces. Figure 4.1 shows a schematic of the Knudsen flow through a straight cylindrical tube with an arbitrary length $L$ and a diameter $d\,(= 2a)$. The tube is connected to a reservoir at $z = -L/2$ containing molecules of a low concentration $n_1$ in an equilibrium state, and the flow through the tube does not disturb the equilibrium. At $z = +L/2$, vacuum conditions exist by setting $n_2 = 0$ (purely for mathematical convenience) so that no flow is returning from this region to the tube interior. This setup originates from the fact that the KD coefficient with an infinite $\lambda$ does not significantly depend on molecular concentration and pressure gradients, but only on the tube geometry. This theory deals with the net molecular flux across the cross-section so that an addition of an arbitrary reference (positive) concentration $n_0$ at each side of the tube, i.e., $n\,(z = -L/2) = n_1 + n_0$ and $n\,(z = L/2) = 0 + n_0$, does not change the theoretical results. Setting $n_0 = 0$ provides a noticeable mathematical simplicity.

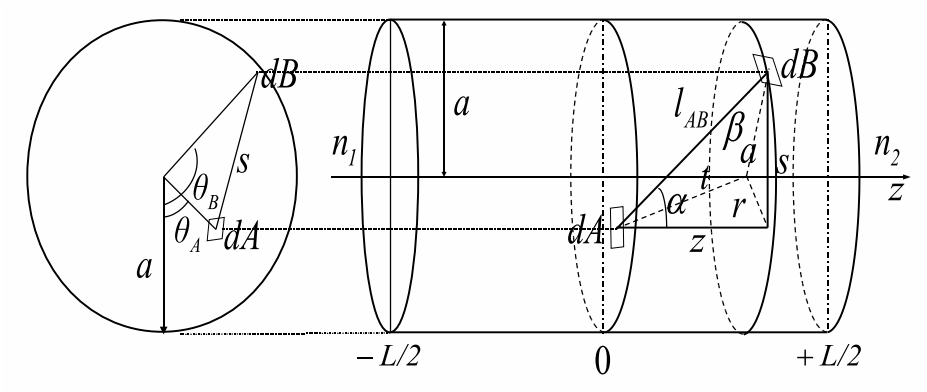


Figure 4.1. Schematic of straight round cylindrical tube of length $L$ and radius $a$. Clausing [4, 5] and Pollard & Present [19] used axial ranges of $0 < z < L$ and $-L/2 < z < +L/2$, respectively.

The number of molecules, $\mathrm{d}N_w$, coming from an element $\mathrm{d}B$ of the tube wall and passing through an infinitesimal cross-sectional area $\mathrm{d}A$ at the center of the tube per unit time, is given by using the classical molecular kinetic theory [21] as

$$-\mathrm{d}N_w = n\,(z)\,\bar{v}\frac{(\mathrm{d}A\cos\alpha)\,(\mathrm{d}B\cos\beta)}{4\pi l_{AB}^2} \tag{4.1.2}$$

where $n\,(z)$ is the molecular number concentration at the position $z$ inside the tube, $l_{AB}$ is the distance between $\mathrm{d}A$ and $\mathrm{d}B$, and $\alpha$ and $\beta$ are angles between $l_{AB}$ and normal directions to $\mathrm{d}A$ and $\mathrm{d}B$, respectively. The following geometrical relationships are used: $\mathrm{d}A = r\,\mathrm{d}r\,\mathrm{d}\theta_A$, $\mathrm{d}B = a\,\mathrm{d}z\,\mathrm{d}\theta_B$, $\cos\alpha = z/l_{AB}$, $\cos\beta = \left(l_{AB}^2 + a^2 - t^2\right)/2al_{AB}$, $l_{AB}^2 = r^2 + a^2 - 2ra\cos\left(\theta_A - \theta_B\right) + z^2$, and $t^2 = r^2 + z^2$. Integrating Eq. (4.1.2) over the central cross-section and whole internal wall surfaces yields

$$-N_w = \frac{\bar{v}}{4\pi}\int_A \mathrm{d}A \int_B \mathrm{d}B\,n\,(z)\,\frac{z\left[a - r\cos\left(\theta_A - \theta_B\right)\right]}{\left[z^2 + a^2 + r^2 - 2ra\cos\left(\theta_A - \theta_B\right)\right]^2} \tag{4.1.3}$$

where

$$\int_A \mathrm{d}A = \int_0^{2\pi}\mathrm{d}\theta_A\int_0^a r\mathrm{d}r \qquad \text{and} \qquad \int_B \mathrm{d}B = \int_0^{2\pi}\mathrm{d}\theta_B\int_{-L/2}^{+L/2}\mathrm{d}z \tag{4.1.4}$$

In order to calculate for $N_w$, the concentration profile $n\,(z)$ should be available. Following PP's work [19], we assume that the molecular concentration linearly decreases from the (left) inlet to the (right) outlet sections:

$$n\,(z) = \frac{n_1}{2} + \left(\frac{\mathrm{d}n}{\mathrm{d}z}\right) z \tag{4.1.5}$$

where $\mathrm{d}n/\mathrm{d}z = -n_1/L$ is a constant. Now, Eq. (4.1.5) is substituted into Eq. (4.1.3) to yield

$$-N_w = 2\bar{v}a\left(\frac{\mathrm{d}n}{\mathrm{d}z}\right)\int_0^a r\mathrm{d}r\int_0^{L/2}\mathrm{d}z\int\mathrm{d}\theta\frac{z^2\left[a - r\cos\left(\theta_A - \theta_B\right)\right]}{\left[z^2 + a^2 + r^2 - 2ra\cos\left(\theta_A - \theta_B\right)\right]^2} \tag{4.1.6}$$

where the term of $n_1/2$ in the integral vanishes by symmetry. We consider the relative angle $\theta_{AB} = \theta_A - \theta_B$ and replace the integration with respect to $\theta_A$ by $2\pi$. This is because a rotation of $\mathrm{d}A$ in the azimuthal direction in Figure 4.1 does not change the result of the angular integration with respect to $\theta_B$. In addition, due to the planar symmetry, integration over $\theta_B$ from $0$ to $\pi$ should be equal to that from $\pi$ to $2\pi$. For simplicity, we set $\theta = \theta_A + \pi$. Eq. (4.1.6) is integrated with respect to $\theta$ from $0$ to $\pi$ and $r$ from $0$ to $a$:

$$N_w = \pi a^2\nu\int_0^{L/2}\frac{1}{a^2}\left[\sqrt{z^2 + 4a^2} + \frac{z^2}{\sqrt{z^2 + 4a^2}} - 2z\right]\frac{z}{L}\mathrm{d}z \tag{4.1.7}$$

where

$$\nu = \frac{1}{4}\bar{v}L\left(-\frac{\mathrm{d}n}{\mathrm{d}z}\right) \tag{4.1.8}$$

is the incidence rate of gas molecules striking the tube wall. Integration of Eq. (4.1.7) over $z$ for the half tube due to symmetry finally provides

$$\eta_{\mathrm{ind}}^{SKL} \equiv \frac{N_w}{\pi a^2\nu} = \frac{4}{3}\left(\frac{d}{L}\right)\left[1 - \frac{1}{4}\left(\frac{L}{d}\right)^3 + \frac{1}{4}\left(\left(\frac{L}{d}\right)^2 - 2\right)\sqrt{\left(\frac{L}{d}\right)^2 + 4}\right] \tag{4.1.9}$$

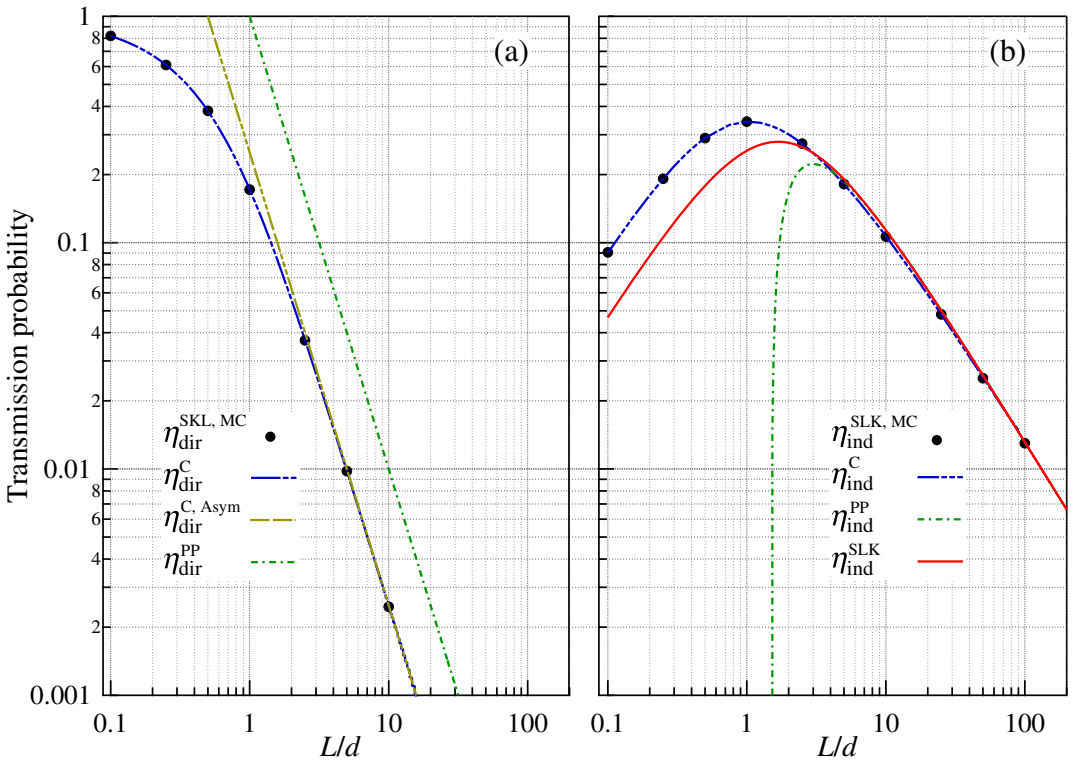


Figure 4.2. Comparison of (a) direct and (b) indirect transmission probabilities vs. dimensionless tube length $L/d$.

where superscript "SKL" indicates initials of the authors' last names. Note that this analytic solution for the indirect TP only assumes the linear concentration profile for low-pressure gases, and we believe that Eq. (4.1.9) is an unprecedented mathematical achievement.

We also calculated the direct and indirect TP through the conventional cylindrical tube using the Monte Carlo method and reproduced results of Talley and Whitaker [27], which should be identical to Clausing's exact solutions. A fourth assumption to those in our theory (discussed above) is that (4) molecules have equal chance of entering at any inlet point of the tube, arriving with an orientation distribution according to the cosine law.

Figure 4.2 compares the direct and indirect TPs of various theoretical approaches and our Monte Carlo simulations (which is basically a reproduction of Talley and Whitaker's work [27]). Figure 4.2(a) shows, first of all, that our Monte Carlo simulation ($\eta_{\rm dir}^{SKL,\,\rm MC}$) and Clausing's direct TP ($\eta_{\rm dir}^{C}$) perfectly match each other, as also indicated for the indirect

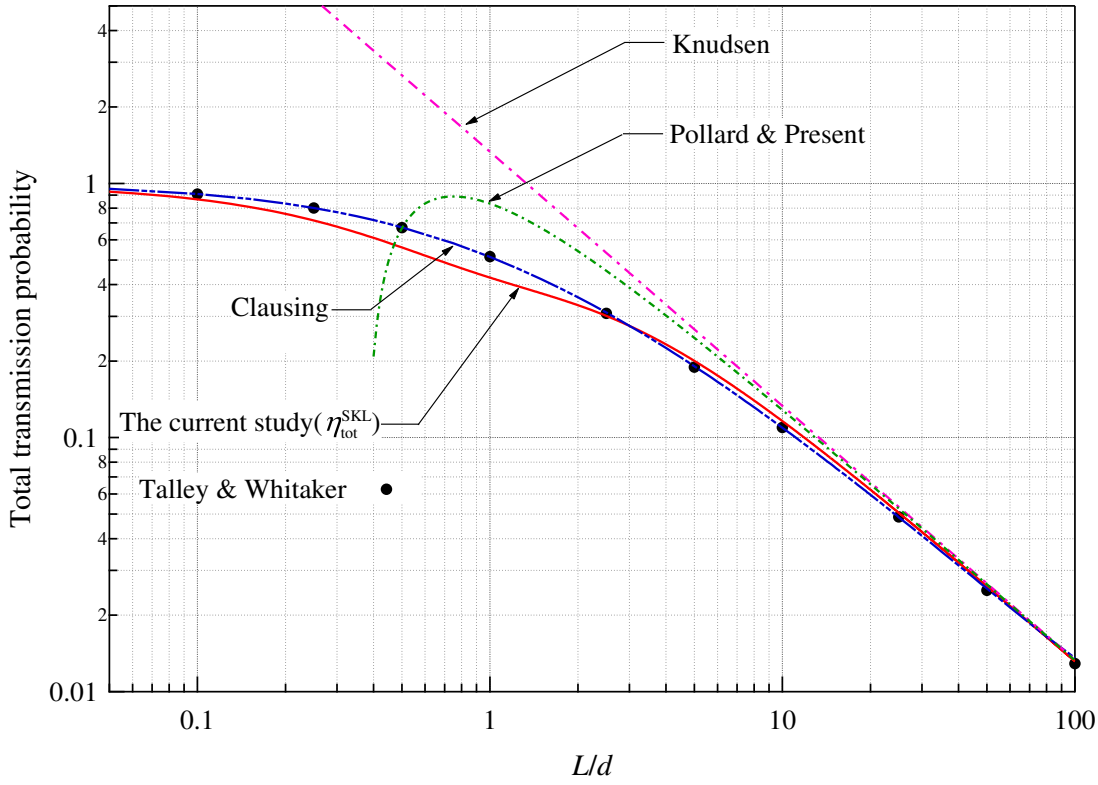


Figure 4.3. Total transmission probability vs. dimensionless tube length $L/d$. Clausing's integral equation theory and Talley and Whitaker's Monte Carlo simulations were reproduced by us. Equations used for Knudsen's and Pollard & Present's graphs are $\eta_{\rm ind}^{K}$ and $\eta_{\rm tot}^{PP}$, respectively.

TPs of $\eta_{\rm ind}^{C}$ and $\eta_{\rm ind}^{SKL,\,\rm MC}$ in Figure 4.2(b). The asymptotic form of Clausing's direct TP ($\eta_{\rm dir}^{C,\,\rm Asym}$) agrees well with the exact solution $\eta_{\rm dir}^{C}$ for $L \gtrsim 2d$ and as indicated above, PP's approximation of the direct TP ($\eta_{\rm dir}^{PP}$) provides fourfold overestimation of $\eta_{\rm dir}^{C,\,\rm Asym}$. Figure 4.2(b) indicates that our analytic solution for the indirect TP ($\eta_{\rm ind}^{SLK}$) is superior to that of the original PP's theory ($\eta_{\rm ind}^{PP}$) especially for short tubes whose lengths are of an order of the diameter or shorter.

The total TP, $\eta_{\rm tot}^{SKL}$, as a sum of direct (of Eq. (4.1.1)) and indirect (of Eq. (4.1.9)) TPs are plotted in Figure 4.3 as compared with Knudsen's, Clausing's, and PP's theoretical results, and our Monte Carlo simulations. As expected from results shown in Figure 4.2, Clausing's exact solution and the Monte Carlo simulation agree very well, and our analytic

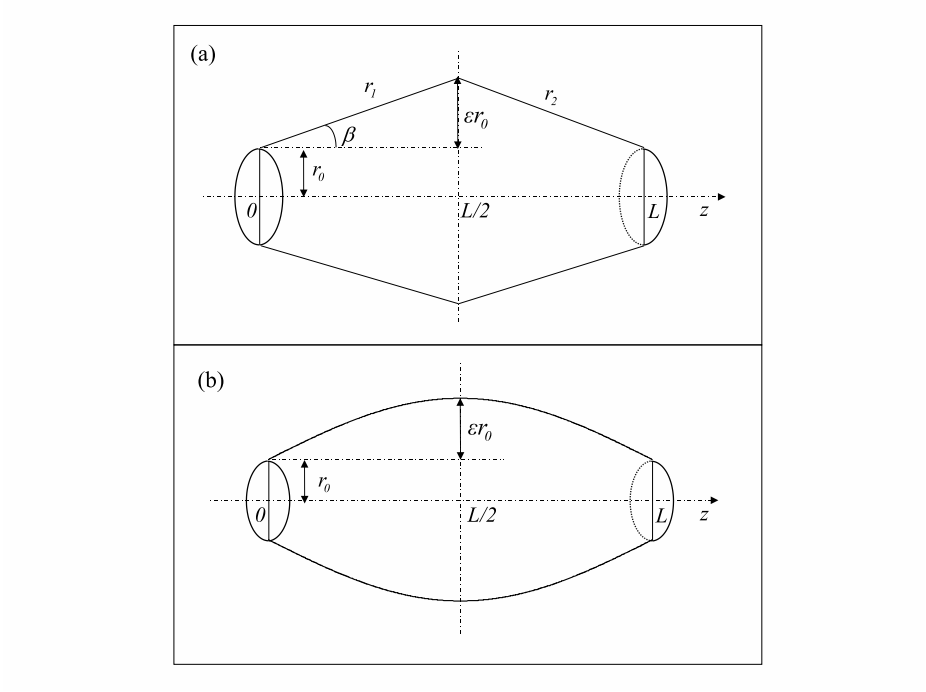


Figure 4.4. Schematic of (a) a diverging-converging and (b) bulging tubes.

solution provides the closest approximation to Clausing's exact solution in comparison to Knudsen's original work and PP's theoretical improvement. Theoretical and simulation results developed in this study are a marginal analytic development and a numerical reproduction of previous research papers, respectively. In the next section, we will use the same approaches to investigate KD phenomena through tubes with structural variation from the straight cylinder.

## 4.2 Diverging-Converging Tube

### 4.2.1 Approximation Analysis

KD phenomena through converging, diverging, and converging-diverging tubes were previously scrutinized by Tally and Whitaker [27]. To the best of our knowledge, however, the (conically) diverging-converging tube (as shown in Figure 4.4(a)), such as two head-cut conical tubes connecting their wider mouths, was not investigated for gas transport

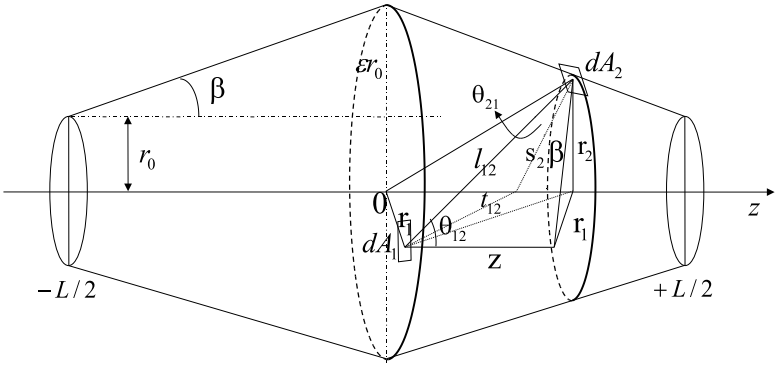


Figure 4.5. Schematic of a divering-converging tube of length $L$ and radius $a$.

in the Knudsen regime. Radii of the left and right side of conical tubes are expressed as a function of the distance from the inlet:

$$r\left(z\right)_{\mathrm{div-conv}} = \begin{cases} r_1 = r_0 + \epsilon\dfrac{2r_0}{L}z, & 0 \le z \le \dfrac{L}{2} \\ r_2 = r_0 + \epsilon\dfrac{2r_0}{L}\left(L - z\right), & \dfrac{L}{2} < z \le L \end{cases} \tag{4.2.1}$$

and the magnitude of angle $\beta$ at the inlet (and outlet) is related to $\epsilon$, i.e., the dimensionless distance from the imaginary tube surface of radius $r_0$ at the mid-point (at $z = L/2$) to the peak of the diverging-converging tube $r_0 + \epsilon r_0$: $\tan\beta = 2\epsilon a/L$. From the definition of Eq.(4.0.1), the equivalent diameter of the conically diverging-converging tube is calculated as

$$d_{\mathrm{eq}}^{\mathrm{div-conv}} = 2r_0\sqrt{1 + \epsilon + \frac{1}{3}\epsilon^2} \tag{4.2.2}$$

In this section, we also developed an analytical solution for a diverging-converging tube by the same method described in section (4.1). Similarly, the total TP for a diverging-converging tube consists of two parts, direct TP ($\eta_{\mathrm{dir}}$) and indirect TP ($\eta_{\mathrm{ind}}$). $\eta_{\mathrm{dir}}$ is independent of the geometrical configuration and has been given by Eq.(4.1.1). We only focused on the indirect TP. Figure 4.5 shows the diagram of a diverging-converging tube. As discussed in section (4.1), we used the same theory to deal with a diverging-converging tube and subsequent mathematical derivations are also the same, except different geometrical re-

lationships were employed: $\mathrm{d}A_1 = r_1 \mathrm{d}r_1 \mathrm{d}\alpha_1$, $\mathrm{d}A_2 = \dfrac{r_2 \mathrm{d}z \mathrm{d}\alpha_2}{\cos\beta}$, $\cos\theta_{12} = \dfrac{z}{l_{12}}$, $\cos\theta_{21} = \dfrac{l_{12}^2 + s_2^2 - t_{12}^2}{2 l_{12} s_2}$, $l_{12}^2 = r_1^2 + r_2^2 - 2 r_1 r_2 \cos(\alpha_1 - \alpha_2) + z^2$, $t_{12}^2 = r_1^2 + (|z| - r_2 \tan\beta)^2$, $s_2 = \dfrac{r_2}{\cos\beta}$, and $r_2 = r_0 + \dfrac{L}{2}\tan\beta - |z|\tan\beta$. Substituting the geometrical relationship into Eq.(4.1.2) and integrating over the variables yields

$$\eta_{\mathrm{ind}}^{\mathrm{div-conv}} = \eta_{\mathrm{ind}}^{\mathrm{SKL}} + \varepsilon f\left(\frac{L}{d}\right) + O\left(\varepsilon^2\right) \tag{4.2.3}$$

where $L$ is the tube length and $d$ equals to $2r_0$. $\eta_{\mathrm{ind}}^{\mathrm{SKL}}$ stands for the indirect TP for a cylindrical tube given by Eq.(4.1.9) and $f\left(\dfrac{L}{d}\right)$ is expressed to be

$$f\left(\frac{L}{d}\right) = \frac{d}{L}\left[4 + \frac{L}{d} + \frac{2d}{L}\ln\left(\frac{2d}{L + \sqrt{L^2 + 4d^2}}\right) - \frac{L^2 + 12d^2}{2d\sqrt{L^2 + 4d^2}}\right] \tag{4.2.4}$$

Therefore, the total TP is the sum of Eqs.(4.1.1) and (4.2.3). Two limiting cases of sufficiently short and long tubes were also investigated as shown in the following:

$$\lim_{L\to 0} \eta_{\mathrm{tot}}^{\mathrm{div-conv}} = \lim_{L\to 0} \eta_{\mathrm{tot}}^{\mathrm{SKL}} + \varepsilon\left(\frac{1}{2} + \frac{L}{6d}\right) \tag{4.2.5}$$

$$\lim_{L\to \infty} \eta_{\mathrm{tot}}^{\mathrm{div-conv}} = \lim_{L\to \infty} \eta_{\mathrm{tot}}^{\mathrm{SKL}} + \varepsilon\frac{4d}{L} \tag{4.2.6}$$

Figure 4.6 shows the total TP of the diverging-converging tube calcualated using the approximate analysis, integral equation theory and Monte Carlo simulations, compared with that of the equivalent straight tube. All tubes have the same internal volume. Comparing the total TP of the cylindrical tube with that of diverging-converging tube, by whatever simulation or approximate analysis, it was found that the TP for the diverging-converging tube is always greater than that of the straight tube, unless the tube length is comparable to the diameter. Figure 4.6 also shows that all three methods have the same trend along the tube length, but the curve of the approximate solution surpassed both integral equation theory and Monte Carlo simulations.

For the approximate analysis, we found it gives us a fatal error in the region of the short tube in which the tube length is less than or comparable to the tube diamter

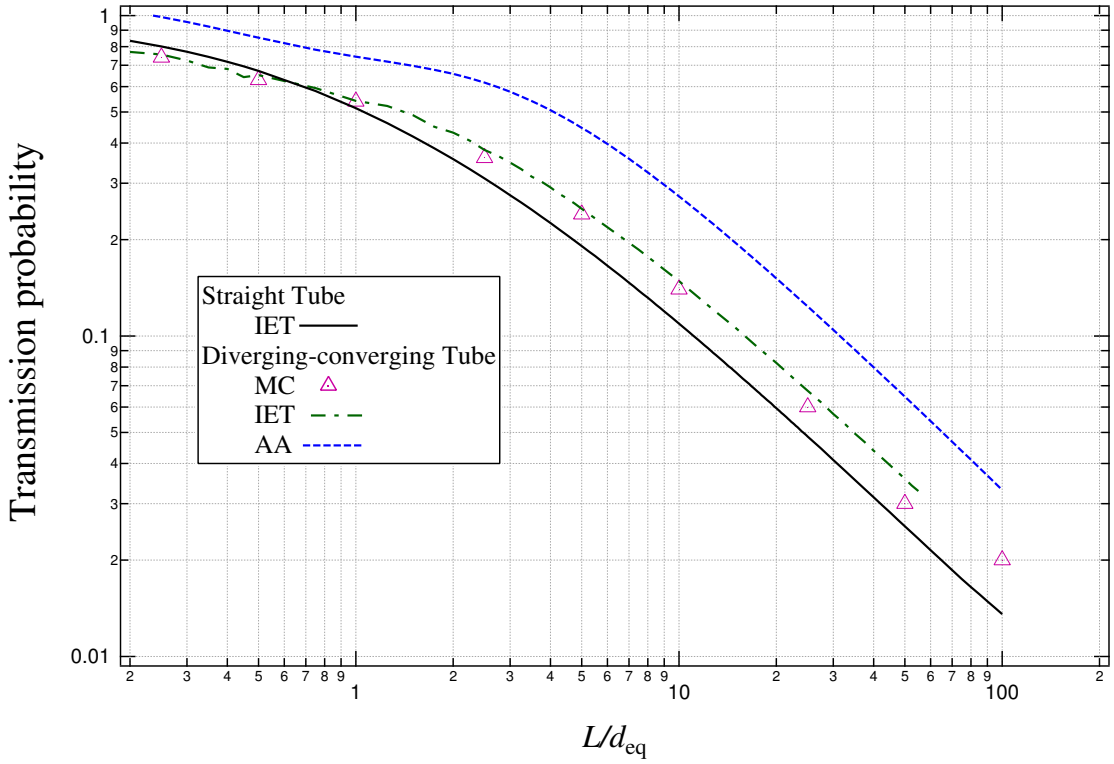


Figure 4.6. Total transmission probability of the diverging-converging tube vs. the dimensionless tube length ($L/d$) with $\epsilon = 0.5$, calculated using approximate analysis (AA), integral equation theory (IET) and Monte Carlo (MC) simulations, as compared with Clausing's exact solution for the cylindrical tube. The equivalent diameters of the diverging-converging are calculated using Eq.(4.2.2).

since the total TP is greater than unit. It was therefore concluded that the approximate analysis considered herein for a diverging-converging tube would be applied to qualitatively evaluate the TP only if the tube length is much larger than its diameter. However, the value of the total TP evaluated by the approximate analysis is at least 2-3 times greater than that of the integral equation theory and Monte Carlo simulation. This result indicated that the linear assumption of the concentration profile along the tube length could not precisely describe the molecular flow through the diverging-converging tube even though it works well in the case of the cylindrical tube.

### 4.2.2 Integral Equation Theory

As discussed in Section 3.2, we followed the Clausing integral equation theory to write the TP as shown in Eqs.(3.2.1) and (3.2.2). Specific functional forms of $\omega$-functions are included in Appendix E. We numerically solve the integral equation of Eq.(3.2.1) after the self-consistent solution for $w(z)$ is obtained.

In general, an analytic solution for Eq.(3.2.2) is not available so that a numerical method must be used to calculate $w(z)$ although an approximate expression of closure form can be obtained, as described in Clausing's original work [4, 5]. Rigorously saying, a numerical iterative process should be used to solve for $w(z)$ to a certain accuracy [22]. A typical method is explained as follows [8]. A trial function is chosen for $w(z)$ as typically the first term of Eq.(3.2.2), i.e., $w(y) = \omega_{\mathrm{rs}}(L - y)$, which is then used for the integration of the second term to obtain an updated function $w(z)$. The whole procedure is iterated until an error between two consecutive steps become less than a tolerance. However, this method is conditionally stable and hence diverges in some cases. The numerical stability of $w(z)$ depends on the tube length and the number of integration points. We found that a linear algebraic method is unconditionally stable to calculate $w(z)$. Details of our new solution approach to reproduce Clausing's $w(z)$ function are given in Appendix B. This algebraic method to solve Eq.(3.2.2) for $w(z)$ is to compare our analytic solution and Clausing's original theory.

Figure 4.7 shows the total TP of the diverging-converging and bulging tubes calculated using our integral equation theory and Monte Carlo simulations, compared with

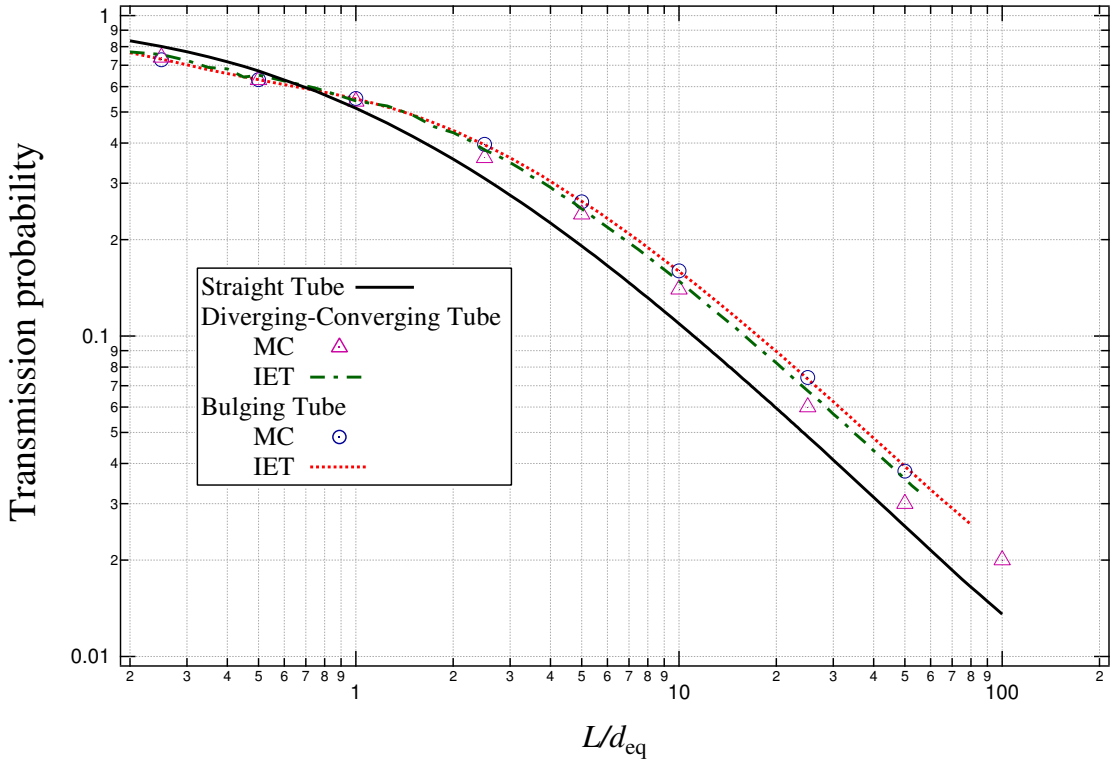


Figure 4.7. Total transmission probability of the diverging-converging and bulging tubes vs. the dimensionless tube length ($L/d$) with $\epsilon = 0.5$, calculated using the integral equation theory (IET) and Monte Carlo (MC) simulations, as compared with Clausing's exact solution. The equivalent diameters of the diverging-converging and bulging tubes are calculated using Eqs.(4.2.2) and (4.3.2), respectively.

that of the equivalent straight tube. All three tubes have the same internal volume and the equivalent radius is the root-mean-square of the radius $r\,(z)$. Unless the tube length is comparable to the diameter, the total TP of a diverging-converging tube is noticeably higher than that of the equivalent straight tube. Davis reported that the converging-diverging tube significantly reduced the TP[6]. We found here that the diverging-converging pore structure near the tube center geometrically pushes entering molecules toward the central region of wider spaces and hence increases the transmission probability. Conversely saying, molecules entered the diverging-converging tube have higher opportunities to move forward to the central regions of the tube and less chance to return to the reservoir. These results will be further discussed in the next section.

## 4.3 Bulging Tube

Now we investigate the molecular transmission through a bulging tube, which is a sinusoidally diverging-converging tube, as shown in Figure 4.4(b). The variation of radii along the axial coordinate from $z = 0$ to $L$ is represented as

$$r\,(z)_{\text{bulging}} = r_0 + \epsilon r_0 \sin\left(\frac{\pi z}{L}\right) \tag{4.3.1}$$

In a similar manner to that of the previous section, the indirect TP is numerically calculated using the Clausing integral equation theory of Eq.(3.2.1). The direct TP, i.e., $\omega_{ss}$, of this case is identical to those of the conventional cylindrical as well as the diverging-converging tubes. We analytically derived three other $\omega$'s for this bulging tube, which are included in Appendix F. The equivalent diameter of this bulging tube is calculated as

$$d_{\text{eq}}^{\text{bulging}} = 2r_0\sqrt{1 + \frac{4}{\pi}\epsilon + \frac{1}{2}\epsilon^2} \tag{4.3.2}$$

Due to the geometrical complexity of this bulging tube, an analytic solution is not available and the Monte Carlo simulations are performed for the bulging pore geometry. Results of our integral equation theory and Monte Carlo simulations are shown in Figure 4.7. The total TPs of the bulging tube is, in general, higher than that of the

diverging-converging tube. Diverging slopes of the two tubes are calculated by derivatives of Eqs.(4.2.1) and (4.3.1) with respect to $z$ at $z = 0$:

$$\left[\frac{\mathrm{d}r\left(z\right)_{\mathrm{div-conv}}}{\mathrm{d}z}\right]_{z=0} = \epsilon\frac{2r_0}{L} = \epsilon\frac{d_{\mathrm{eq}}^{\mathrm{div-conv}}}{L}\frac{1}{\sqrt{1+\epsilon+\frac{1}{3}\epsilon^2}} \tag{4.3.3}$$

$$\left[\frac{\mathrm{d}r\left(z\right)_{\mathrm{bulging}}}{\mathrm{d}z}\right]_{z=0} = \epsilon\left(\frac{\pi}{2}\right)\frac{2r_0}{L} = \epsilon\frac{d_{\mathrm{eq}}^{\mathrm{bulging}}}{L}\frac{\pi/2}{\sqrt{1+\frac{4}{\pi}\epsilon+\frac{1}{2}\epsilon^2}} \tag{4.3.4}$$

The ratio of Eqs.(4.3.4) to (4.3.3) indicate that for small $\epsilon$ the bulging tube has an inlet slope as much as $\pi/2$ times as higher than that of the diverging-converging tube with the same equivalent diameter. This implies that the geometrical slope at the inlet noticeably increases the total TP as compared to that of the equivalent straight tube. For filtration processes the pore sizes should be small enough to reject solute ions or particles, but larger void spaces that provide diversing slopes at the pore inlet can enhance the solvent transport through membranes.

## 4.4 Periodic Tube

Transmission probability of periodic tubes is investigated using the Monte Carlo method for pore structures which are divided into two groups, positive and negative cosinusoidal tubes, as described by

$$r(z)_{\mathrm{periodic}} = r_0 \pm \epsilon r_0 \cos\left(\frac{2m\pi z}{L}\right) \tag{4.4.1}$$

where $m$ is the periodicity coefficient. Figure 4.8 shows the pore structures of $m = 1$ and $\epsilon = \pm 0.5$. The tube slope at the inlet is zero because the cosine function has a maximum and minimum at every half period, $L/2$. The equivalent diameter of this periodic tube (independent of the periodicity coefficient $m$) is given as

$$d_{\mathrm{eq}}^{\mathrm{periodic}} = 2r_0\sqrt{1+\epsilon^2/2} \tag{4.4.2}$$

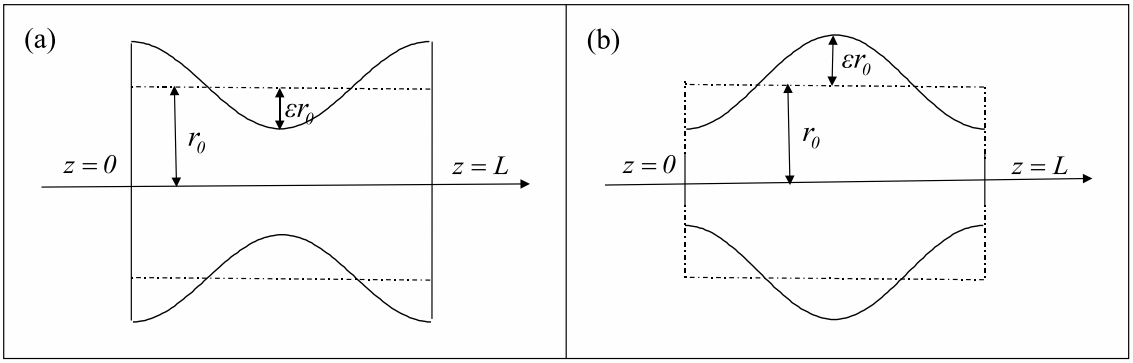


Figure 4.8. Schematic of (a) positive and (b) negative cosinusoidal tubes. The pore shape was described by (a) $r\left(z\right) = r_0 + \epsilon r_0 \cos\left(\frac{2\pi z}{L}\right)$ and (b) $r\left(z\right) = r_0 - \epsilon r_0 \cos\left(\frac{2\pi z}{L}\right)$ with $m = 1$. Functions used in (a) and (b) have a phase difference of $L/2$ with respect to $z$ .

which indicates that the equivalent diameter is (slightly) greater than $2r_0$ because the second order of $\epsilon$ has only a minimal influence. We calculate the inlet slope at the first location where the tube radius is equal to the base line of the imaginary tube, i.e., at $z = L/4m$ as

$$\left[\frac{\mathrm{d}r\left(z\right)_{\mathrm{periodic}}}{\mathrm{d}z}\right]_{z=L/4m} = \pm\epsilon r_0 \frac{2m\pi}{L} = \pm\epsilon \frac{d_{\mathrm{eq}}^{\mathrm{periodic}}}{L} \frac{m\pi}{\sqrt{1+\epsilon^2/2}} \tag{4.4.3}$$

so that as $m$ increases the diverging/converging slope of the positive/negative cosinusoidal tube increases in magnitude accordingly.

Davis [6] implied that if a block exists in the middle of a tube, then the TP decreases. We also found that the positive cosinusoidal tube does not provide for any cases of $m$, $\epsilon$, and $L/d$, a TP higher than that of the equivalent tube so that we confined ourselves to negative cosinusoidal tubes only. Figure 4.9 shows the total TPs of the negative cosinusoidal tubes versus the dimensionless tube length, i.e., the length divided by the equivalent diameter, with $\epsilon = 0.5$ and various periodicity coefficients: (a) log-long and (b) semi-log scales. Since we used integer $m$ values of 1, 5, 25, 50, and 500, the equivalent diameters used in Figure 4.9 are all identical. As $m$ increases, the crossing point is farther from the tube inlet. It is interesting to observe in Figure 4.9(a) that each TP curve with specific $m$

crosses that of the equivalent straight tube. Specifically for this case of $\epsilon = 0.5$, the crossing points measured as $L/d_{\mathrm{eq}}$ are very close to the periodicity coefficient $m$. The ratio plot of Figure 4.9(b), i.e., the TP of the negative cosinusoidal tube normalized by that of the equivalent straight tube, clearly shows this trend: the crossing points of $m$ =1, 5, 25, and 50 are roughly estimated as $L_{\mathrm{cross}}/d_{\mathrm{eq}}$= 1.1, 7.0, 40, and 80. The Monte Carlo simulations for $L/d \geqq 1,000$ took an unreasonably long time (more than a few weeks), but the general trend of Figure 4.9(b) for $m = 500$ indicates the ratio can exceed 1.0 near $L/d = 1,000$.

We did some Monte Carlo simulations with $\epsilon = 0.25$ so that the negatively cosinusoidal tubes have less geometrical curvature on the lateral side. Simulation results are shown in Figure 4.10(a) and (b) for log-log and semi-log plots, respectively. Figure 4.10(a) shows the identical trend to that of Figure 4.9(a), but the TP curves of various $m$ are closer to that of the equivalent straight tube, which results in shorter crossing points after which the TPs of the negatively cosinusoidal tubes exceed that of the equivalent straight tube. For $m$ = 1, 5, 25, and 50 $L_{\mathrm{cross}}/d_{\mathrm{eq}}$ values are roughly estimated from the ratio plot of Figure 4.10(b) as 0.9, 5, 22, and 50, which are smaller than the corresponding values of the $\epsilon = 0.5$ case, but surprisingly close to the $m$ values used.

Our objective of this research is to find out optimal geometry of long straight tube by periodically changing the tube diameter. A high value of $\epsilon$ close to 1.0 will cause a deleteriously hampering effect on the molecular transport so that we confined ourselves to small $\epsilon \leq 0.5$. Figures 4.9 and 4.10 provide significant engineering implications. First, it is understood that any structural changes from the conventional straight, round cylindrical tube hamper the Knudsen transport by effectively blocking molecular movements from the inlet to the outlet so that the TP decreases. The only exceptions were the (linearly) diverging-converging tube and slot. If a periodicity characterized by $m$ is implemented in the tube radius along the length, then the TP of the periodic tube exceeds that of the equivalent straight tube near $L_{\mathrm{cross}}/d_{\mathrm{eq}}$ or after. A higher amplitude of the periodicity, $\epsilon$, increases the TP of the periodic tube as much as 1.5 times, estimated visually from Figures 4.9 and 4.10, but the trade-off is a longer dimensionless crossing distance $L_{\mathrm{cross}}/d_{\mathrm{eq}}$ at which the TP ratio becomes unity. The optimal geometry for the maximum TP seems to be dependent on the dimensionless tube length; however, if the periodicity coefficient is about an order of magnitude less than the dimensionless tube length, the TP reaches its maximum

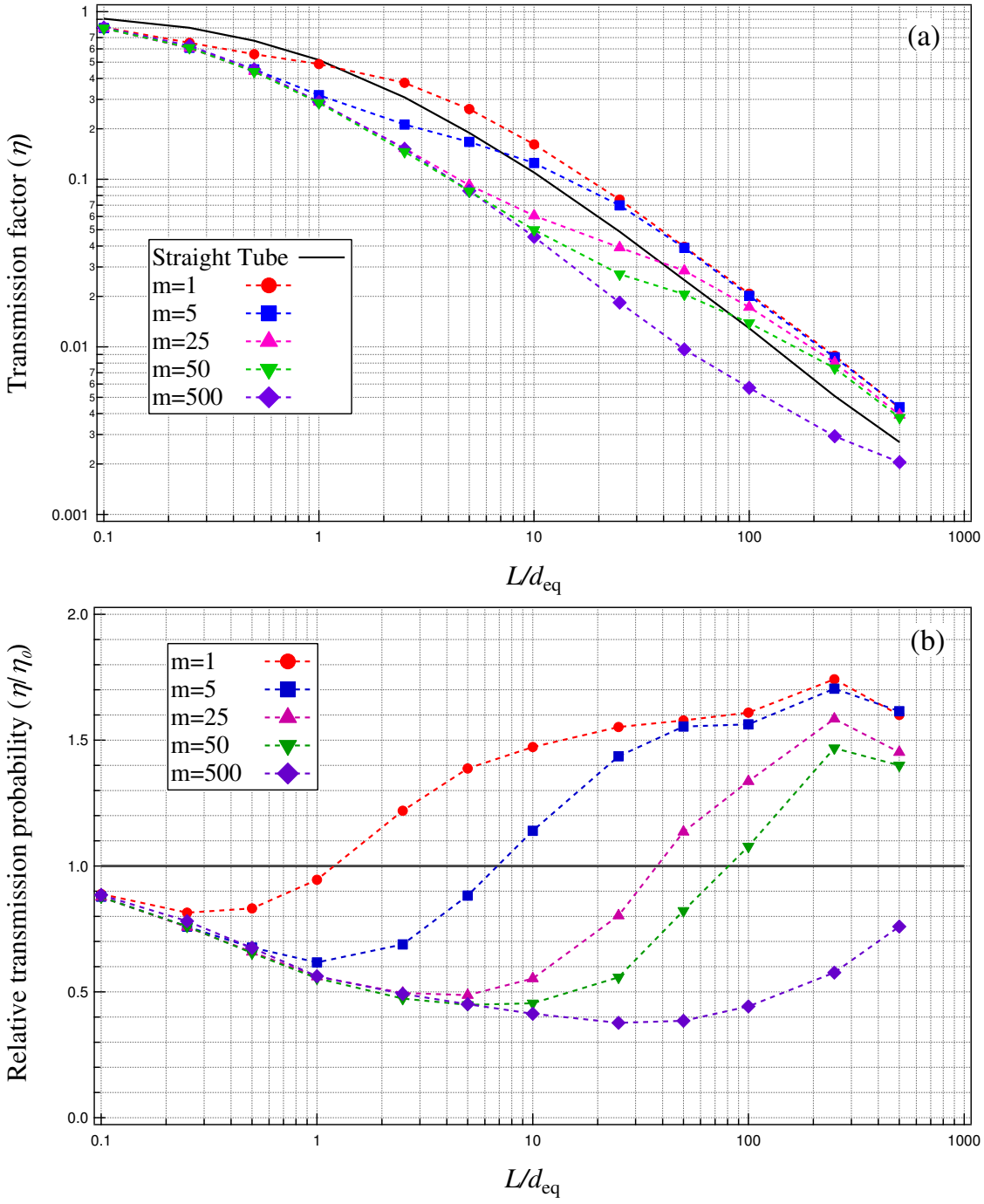


Figure 4.9. Total transmission probability of a periodic, negative cosinusoidal tube with $\epsilon = 0.5$ versus the dimensionless tube length $L/d_{\text{eq}}$: (a) log-log and (b) semi-log plots.

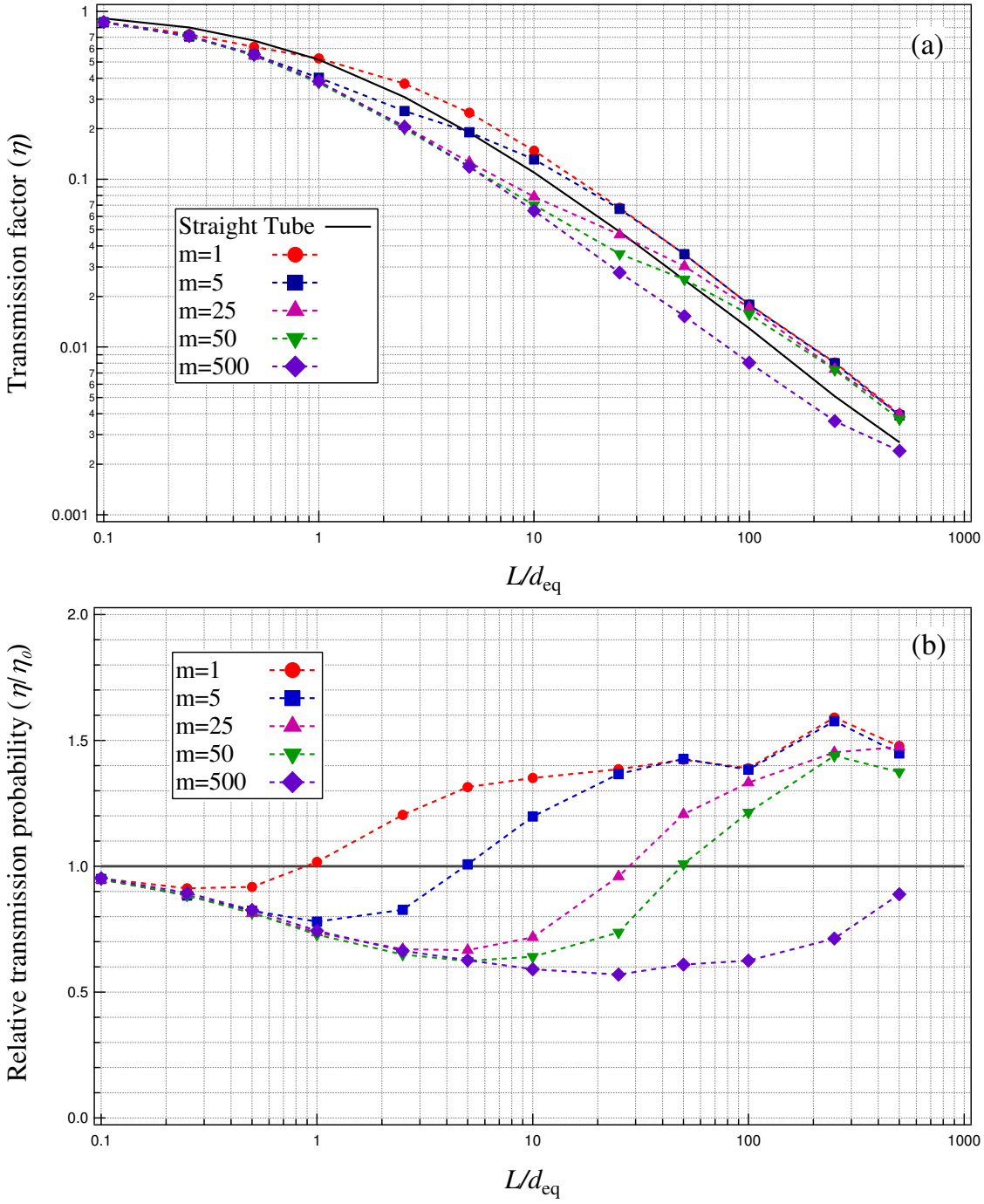


Figure 4.10. Total transmission probability of a periodic, negative cosinusoidal tube with $\epsilon = 0.25$ versus the dimensionless tube length $L/d_{\text{eq}}$: (a) log-log and (b) semi-log plots.

value. From Figures 4.9(b) and 4.10(b) (for cases of $m = 1$ and 5), the maximum TP ratios are roughly estimated as 1.6 and 1.4, respectively.

## 4.5 Effects of Various Internal Structures on TP

In this section, the effect of various internal structures on the transmission probability was investigated using Monte Carlo simulations and the results were compared with the cylindrical tube keeping the same length and internal void volume. Figure 4.11. shows three different internal structures, i.e., (a) convex, (b) linear and (c) concave bulging tubes. The variation of radii along the longitudinal direction from $z = 0$ to $L$ and the corresponding equivalent diameter according to Eq. (4.0.1) are expressed in the following section:

1. Convex-bulging tube

$$r(z)_{\text{convex}} = r_0 + \left| \varepsilon r_0 \sin \frac{2\pi}{L} z \right| \tag{4.5.1}$$

$$d_{\text{eq}}^{\text{convex}} = 2r_0 \sqrt{1 + \frac{4}{\pi}\varepsilon + \frac{1}{2}\varepsilon^2} \tag{4.5.2}$$

2. Concave-bulging tube

$$r(z)_{\text{concave}} = r_0 + \varepsilon r_0 \left( 1 - \left| \cos \frac{2\pi}{L} z \right| \right) \tag{4.5.3}$$

$$d_{\text{eq}}^{\text{concave}} = 2r_0 \sqrt{\frac{3\varepsilon^2 + 4\varepsilon + 2}{2} - \frac{4\varepsilon(1+\varepsilon)}{\pi}} \tag{4.5.4}$$

3. Linear-bulging tube

$$r\,(z)_{\text{linear}} = \begin{cases} r_1 = r_0 + \epsilon r_0 \dfrac{4z}{L}, & 0 \le z \le \dfrac{L}{4} \\ r_2 = (1+2\varepsilon) r_0 - \epsilon r_0 \dfrac{4z}{L}, & \dfrac{L}{4} < z \le \dfrac{L}{2} \\ r_3 = (1-2\varepsilon) r_0 + \epsilon r_0 \dfrac{4z}{L}, & \dfrac{L}{2} < z \le \dfrac{3L}{4} \\ r_3 = (1+4\varepsilon) r_0 - \epsilon r_0 \dfrac{4z}{L}, & \dfrac{3L}{4} < z \le L \end{cases} \tag{4.5.5}$$

$$d_{\text{eq}}^{\text{linear}} = 2r_0 \sqrt{1 + \varepsilon + \frac{1}{3}\varepsilon^2} \tag{4.5.6}$$

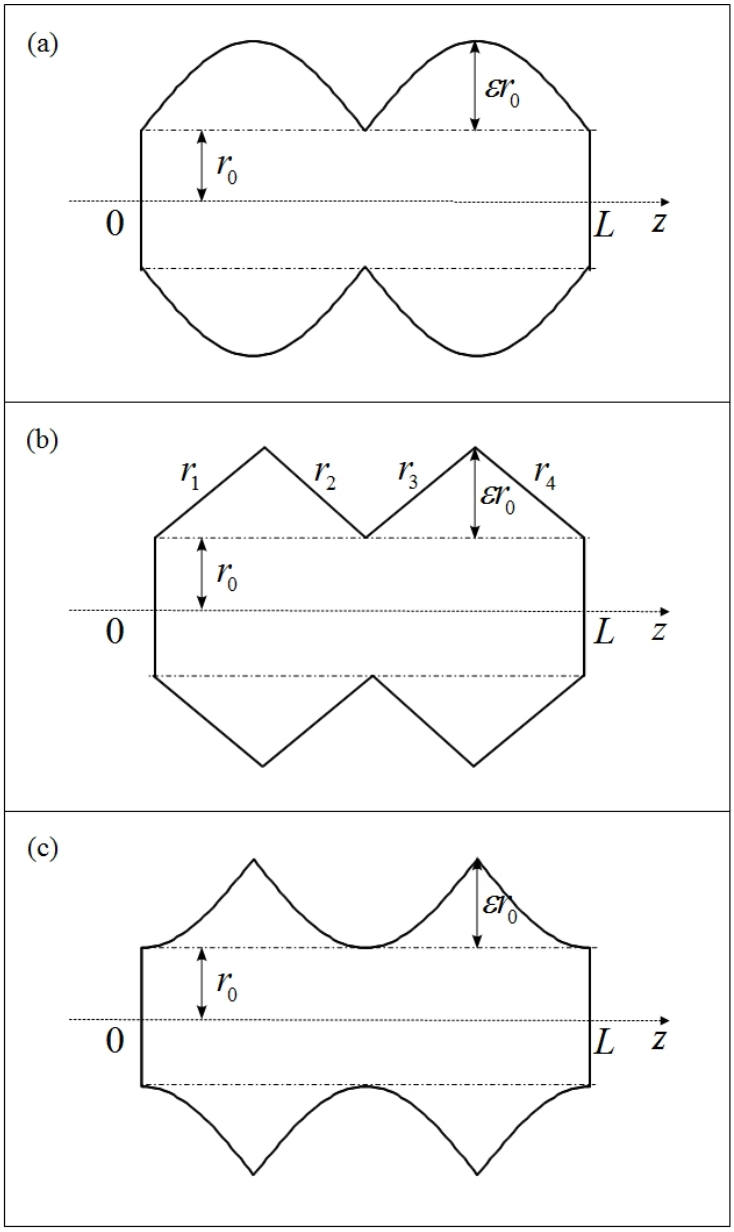


Figure 4.11. Schematic of different internal structures (a) convex, (b) linear and (c) concave bulging tubes.

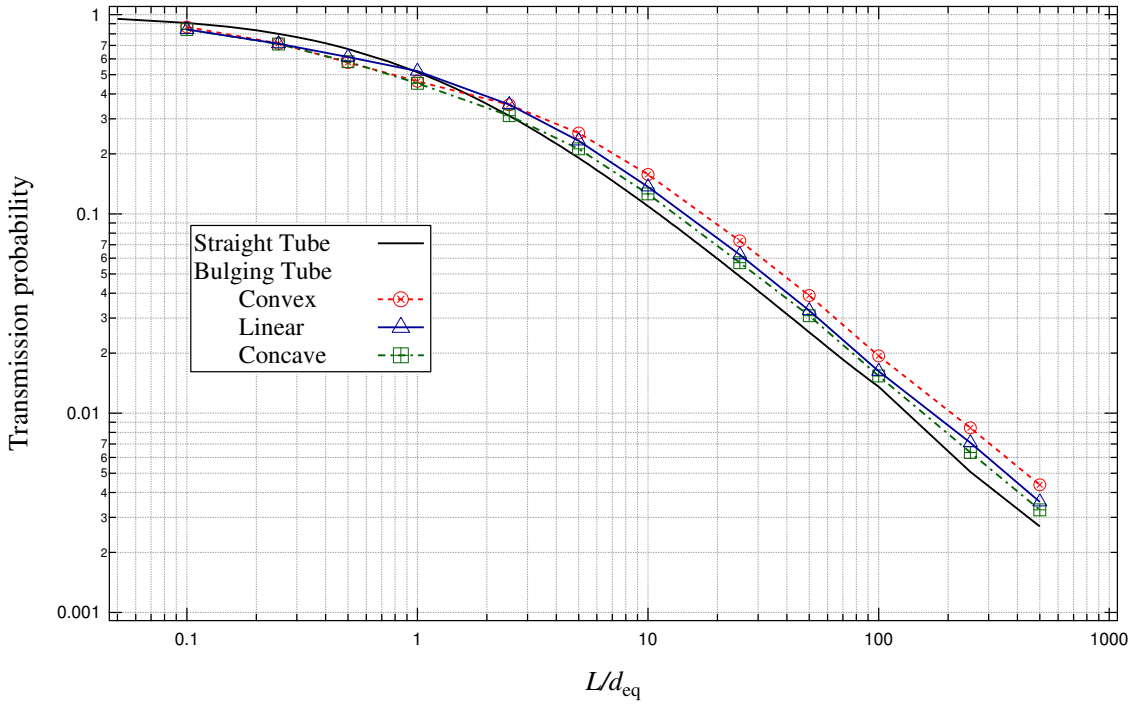


Figure 4.12. Total transmission probability of three different internal structures, i.e., convex, linear and concave tubes, vs. the dimensionless tube length ($L/d$) with $\epsilon = 0.5$, calculated using Monte Carlo (MC) simulations , as compared with the straight tube using the Clasing's exact solution. The equivalent diameters of convex, linear and concave tubes are calculated using Eqs. (4.5.2), (4.5.4) and (4.5.6), respectively.

As discussed in section 3.3, the derivation of $r(z)$ have to be calculated to determine the direction cosines after each collision with the tube wall during the process of the Monte Carlo simulation. It is noted that Eq. (4.5.5) could be rewritten in Fourier series

$$r(z)_{\text{linear}} = r_0 + \varepsilon r_0 \left[ \frac{1}{2} - \frac{4}{\pi^2} \left( \frac{\cos \frac{4\pi}{L} z}{1^2} + \frac{\cos \frac{4\pi}{L} 3z}{3^2} + \frac{\cos \frac{4\pi}{L} 5z}{5^2} + \cdots \right) \right] \tag{4.5.7}$$

which would be more convenient for the derivative calculation than Eq. (4.5.5).

Due to the complexity of these bulging geometries, both analytical approximation and integral equation theory could not be developed to determine the TP and therefore Monte Calo simulations were employed to calculate the TP in this case. The internal void

volume of three different geometries was kept same during the calculation and their corresponding factor of the equivalent diameter to the straight tube are given by Eqs. (4.5.2), (4.5.4) and (4.5.6), respectively. Figure 4.12 shows the TP for three different internal structures as a function of the dimensionless tube length and as well as the straight tube. As we discussed in the preceding sections, the TP for a bulging tube is always higher than that of the equivalent staight tube when the tube length is much greater than its diameter. This conclusion is also confirmed by Fig. 4.12. Here we classified the tube length into two regions for the convenience of the discussion. One is the tube length comparable to the its diameter. In this case, it is found that the TP of these three bulging tubes is below that of the equivalent straight tube, which is consistent with the previous discussion as shown in Fig. 4.7. Another is the tube length much greater than its diameter. In this region, however, we found that among of these three different internal structures, convex-bulging tubes can be more contributed to the TP than linear-bulging tubes, and than concave-bulging tubes at the same tube length and void volume. Quantitatively, the TP for the convex-bulging, linear-bulging and concave-bulging tubes are about 1.5, 1.3 and 1.2 times greater than that of the equivalent straight tube, respectively. Roughly speaking, we may address the conclusion that the internal structures would have no marked effect on the TP comparing with the effect of different geometris, e.g., the TP would noticeably decline if the tube has a throat in the middle.

# Chapter 5

# Conclusions

In this study, we investigated the direct and indirect transmission probabilities (TPs) through various tube structures using the integral equation theory, standard diffusion theory, and Monte Carlo simulations. We found that the framework of the axial range in the cylindrical coordinates influences the asymptotic representations of the TPs. We derived an analytic solution for the indirect TP using the standard diffusion theory, with which Walsh's exact solution provides a complete solution set for the total TP through a conventional cylindrical tube. The diverging tube with the opening inlet structure noticeably enhances the indirect TPs; and the bulging tube which has a stiffer opening slope gives a higher TP than that of the diverging-converging tube of the same void volume. Periodic tubes show a higher TP than that of the equivalent tube as the dimensionless length exceeds the periodicity coefficient depending on the tube peak-amplitude. For filtration purposes, it is implied that membranes with periodic pore structures along the transport direction can enhance the separation performance as influenced by the molecular mean free path, pore diameter, and pore periodicity.

# Appendix A

# Derivation of $\omega's$

1. $\omega_{rr}(z)\mathrm{d}z$

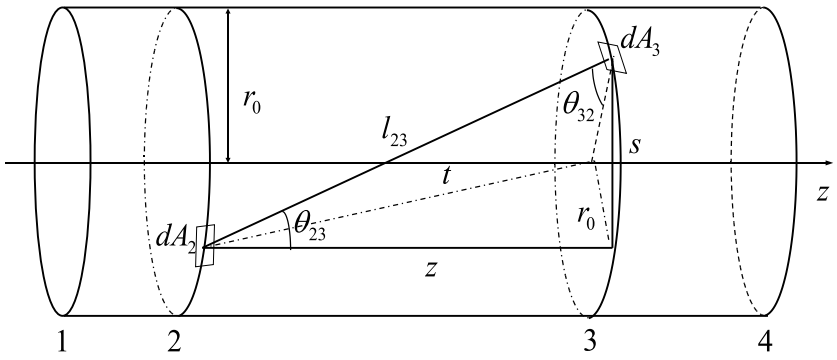


Figure A.1. Schematic illustration of the cylindrical tube for the derivation of $\omega_{rr}(z)\mathrm{d}z$

A diagram of a cylindrical tube with length $L$ and radius $a$ is illustrated in Figure A.1, in which a molecule leaves a ring of an infinitesimal area $\mathrm{d}A_2$, and strikes directly another ring of the area $\mathrm{d}A_3$ located at a distance of $z$. In this section, the inlet and outlet

surface are denoted by 1 and 4, respectively and the ring is represented by 2 and 3 with a distance of $z$.

According to the cosine law, $\omega_{rr}(z)\mathrm{d}z$ can be expressed as

$$\omega_{rr}\left(z\right)\mathrm{d}z=\int_{A_3}\frac{\cos\theta_{23}\cos\theta_{32}}{\pi l_{23}^2}\mathrm{d}A_3 \tag{A.0.8}$$

Following geometrical relationships is applied:

$$\begin{aligned}
&l_{23}^2=z^2+s^2=z^2+2a^2-2a^2\cos\alpha\\
&t^2=a^2+z^2\\
&\cos\theta_{32}=\frac{l_{23}^2+a^2-t^2}{2al_{23}}=\frac{a}{l_{23}}(1-\cos\alpha)\\
&\cos\theta_{23}=\cos\theta_{32}\\
&\mathrm{d}A_3=a\mathrm{d}\alpha\mathrm{d}z
\end{aligned}$$

Substituting above expressions into the Eq.(A.0.14) and integrating over $\alpha$ from $0$ to $2\pi$ yields

$$\begin{aligned}
\omega_{rr}\left(z\right)\mathrm{d}z &= \frac{a^3\mathrm{d}z}{\pi}\int_0^{2\pi}\frac{\left(1-\cos\alpha\right)^2}{\left(z^2+2a^2-2a^2\cos\alpha\right)^2}\mathrm{d}\alpha\\
&= \frac{1}{4a}\left(2+\frac{z^3}{\sqrt{\left(z^2+4a^2\right)^3}}-\frac{3z}{\sqrt{z^2+4a^2}}\right)\mathrm{d}z
\end{aligned} \tag{A.0.9}$$

2. $\omega_{rs}(z)$

A similar diagram was shown in Figure A.2, where a molecule leaving a ring of an infinitesimal area $2\pi a\mathrm{d}z$ between $z$ and $z+\mathrm{d}z$ passes directly through the outlet section of area $\pi a^2$. In terms of the definition, $\omega_{rs}(z)$ can be determined by

$$\omega_{rs}\left(z\right)=\int_{A_4}\frac{\cos\theta_{24}\cos\theta_{42}}{\pi l_{24}^2}\mathrm{d}A_4 \tag{A.0.10}$$

From Figure A.2, we have

$$\begin{aligned}
&l_{24}^2=z^2+s^2=z^2+a^2+r_4^2-2ar_4\cos\alpha\\
&t^2=r_4^2+z^2\\
&\cos\theta_{24}=\frac{l_{24}^2+a^2-t^2}{2al_{24}}=\frac{a-r_4\cos\alpha}{l_{24}}
\end{aligned}$$

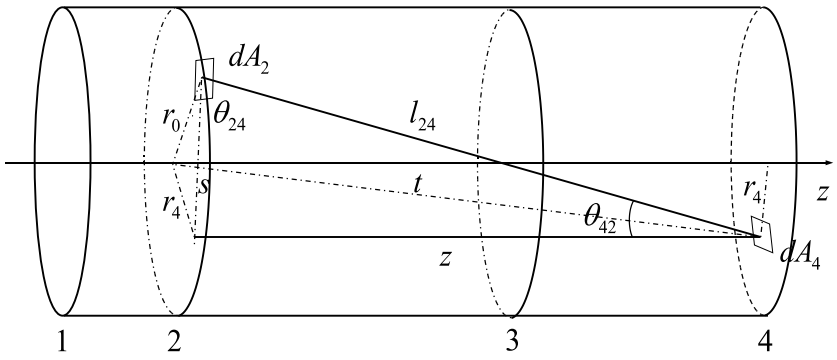


Figure A.2. Schematic illustration of configurations for the derivation of $\omega_{rs}(x)$

$$\cos\theta_{42} = \frac{z}{l_{24}}$$
$$\mathrm{d}A_4 = r_4 \mathrm{d}r_4 \mathrm{d}\alpha$$

Putting the above relationships into the Eq.(A.0.14) and integrating over $\alpha$ from $0$ to $2\pi$ and $r_4$ from $0$ to $a$ gives

$$\begin{aligned}\omega_{rs}(z)\,\mathrm{d}z &= \frac{1}{\pi}\int_0^a r_4 \mathrm{d}r_4 \int_0^{2\pi} \frac{z\,(r - r_4\cos\alpha)}{\left(z^2 + a^2 + r_4^2 - 2ar_4\cos\alpha\right)^2}\mathrm{d}\alpha \\ &= \frac{1}{4a}\left(\sqrt{z^2+4a^2} + \frac{z^2}{\sqrt{z^2+4a^2}} - 2z\right) \end{aligned} \tag{A.0.11}$$

3. $\omega_{sr}(z)\mathrm{d}z$

$\omega_{sr}(z)\mathrm{d}z$ can be defined by the cosine law as

$$\omega_{sr}(z) = \frac{1}{\pi a^2}\int_{A_1}\int_{A_2} \frac{\cos\theta_{12}\cos\theta_{21}}{\pi l_{12}^2}\mathrm{d}A_1\mathrm{d}A_2 \tag{A.0.12}$$

Similar to Figure A.1 and A.2, the geometrical relationships involved the derivation of $\omega_{sr}(z)\mathrm{d}z$ can be described as

$$
\begin{aligned}
&l_{12}^2 = z^2 + s^2 = z^2 + a^2 + r_1^2 - 2ar_1\cos\alpha \\
&t^2 = r_1^2 + z^2 \\
&\cos\theta_{21} = \frac{l_{12}^2 + a^2 - t^2}{2al_{12}} = \frac{a - r_1\cos\alpha_1}{l_{12}} \\
&\cos\theta_{12} = \frac{z}{l_{12}} \mathrm{d}A_1 = r_1 \mathrm{d}r_1 \mathrm{d}\alpha_1 \\
&\mathrm{d}A_2 = a\mathrm{d}z\mathrm{d}\alpha_2
\end{aligned}
$$

Thus, the final expression of $\omega_{sr}(z)\mathrm{d}z$ is obtained by replacing above equations into Eq.(A.0.14) and integrating over the variables as

$$
\begin{aligned}
\omega_{sr}\left(z\right)\mathrm{d}z &= \frac{\mathrm{d}z}{\pi a}\int_0^{2\pi}\mathrm{d}\alpha_2\int_0^a r_1\mathrm{d}r_1\int_0^{2\pi}\frac{z\left(r - r_1\cos\alpha\right)}{\left(z^2 + a^2 + r_1^2 - 2ar_1\cos\alpha\right)^2}\mathrm{d}\alpha \\
&= \frac{1}{2a^2}\left(\sqrt{z^2+4a^2} + \frac{z^2}{\sqrt{z^2+4a^2}} - 2z\right) \qquad \text{(A.0.13)}
\end{aligned}
$$

4. $\omega_{ss}(z)\mathrm{d}z$

Similarly,

$$
\omega_{ss}\left(z\right) = \frac{1}{\pi a^2}\int_{A_1}\int_{A_4}\frac{\cos\theta_{14}\cos\theta_{41}}{\pi l_{14}^2}\mathrm{d}A_1\mathrm{d}A_4 \qquad \text{(A.0.14)}
$$

We have:

$$
\begin{aligned}
&l_{14}^2 = z^2 + s^2 = z^2 + r_1^2 + r_4^2 - 2r_1r_4\cos\alpha \\
&t^2 = r_1^2 + z^2 \\
&\cos\theta_{14} = \frac{z}{l_{14}} \\
&\cos\theta_{41} = \cos\theta_{14} \\
&\mathrm{d}A_1 = r_1\mathrm{d}r_1\mathrm{d}\alpha_1 \\
&\mathrm{d}A_4 = r_4\mathrm{d}r_4\mathrm{d}\alpha_2
\end{aligned}
$$

After substituting those geometrical relationships, Eq.(A.0.14) is eventually integrated to be

$$
\begin{aligned}
\omega_{ss}\left(z\right) &= \frac{1}{\pi a^2}\int_0^a r_4\mathrm{d}r_4\int_0^{2\pi}\mathrm{d}\alpha_4\int_0^a r_1\mathrm{d}r_1\int_0^{2\pi}\frac{z\left(r - r_1\cos\alpha_1\right)}{\left(z^2 + r_4^2 + r_1^2 - 2r_1r_4\cos\alpha_1\right)^2}\mathrm{d}\alpha_1 \\
&= \frac{1}{2a^2}\left(z^2 - z\sqrt{z^2+4a^2} + 2a^2\right) \qquad \text{(A.0.15)}
\end{aligned}
$$

# Appendix B

# Numerical Scheme for Solving Eq.(3.2.2)

Eq.(3.2.2) has a general form of

$$f(x) = g(x) + \int_a^b k(x,y) f(y) dy \tag{B.0.16}$$

where $g\,(x)$ and $k\,(x,y)$ are given and $f\,(x)$ is to be calculated. The integration interval $[a,b]$ is evenly divided into $n$ even sequential sections, of which points are denoted as $x_0$, $x_1$, $x_2$, ..., $x_n$ such as

$$\begin{aligned} x_i &= x_0 + ih \\ h &= \frac{b-a}{n} \end{aligned} \tag{B.0.17}$$

where $i$ =0, 1, 2,... $n$. Then, Eq.(B.0.16) can be expressed as

$$f_i = g_i + h \sum_{j=0}^{n} k_{ij} f_j \tag{B.0.18}$$

and further

$$\sum_{j=0}^{n} \left[\delta_{ij} - k_{ij}\right] f_j = g_j \tag{B.0.19}$$

where $f_i = f\,(x_i)$, $g_i = g\,(x_i)$, $k_{i,j} = k\,(x_i, y_j)$ and $\delta_{ij}$ is Kronecker's delta . In a matrix form,

$$h\,(\boldsymbol{I} - \boldsymbol{k}) \cdot \boldsymbol{f} = \boldsymbol{g} \tag{B.0.20}$$

therefore

$$\boldsymbol{f} = h^{-1} \left( \boldsymbol{I} - \boldsymbol{k} \right)^{-1} \cdot \boldsymbol{g} \tag{B.0.21}$$

This implicit scheme in unconditionally stable and a desired accuracy can be achieved by increasing $n$.

# Appendix C

# Procedures of Monte Carlo Simulation

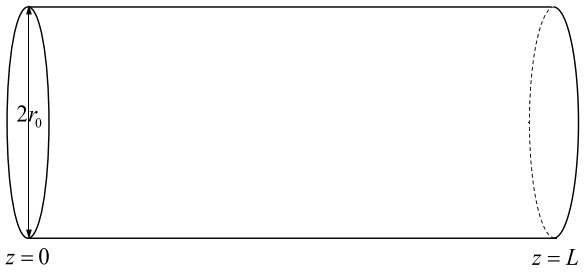


Figure C.1. Schematic illustration of a straight tube with length $L$ and radius $r_0$

The system to be studied is illustrated in Figure C.1. It is assumed that the tube is connected to a low density reservoir at $z = 0$. At $z = L$ we assume the tube is connected to a perfect vacuum so that no molecules enter the tube at $z = L$. Therefore, the TP $\eta$ can be calculated by the definition Eq.(2.1.3).

The calculation depends on one parameter, $L/r_0$, where $L$ is the length of the straight cylindrical tube and $r_0$ is the radius. For convenience in the calculation, $r_0$ is set equal to one. The point of entry is distributed uniformly across the face of the tube provided the flow does not influence the distribution of velocities in the reservoir. A random

coordinate $(x, y, z)$ at the inlet surface is generated by a rejection technique in which two random numbers $\xi_1$ and $\xi_2$ as

$$x_0 = (2\xi_1 - 1) \tag{C.0.22a}$$

$$y_0 = (2\xi_2 - 1) \tag{C.0.22b}$$

$$z_0 = 0 \tag{C.0.22c}$$

The generated coordinate can be accepted only if the condition $x^2 + y^2 \leq 1$ is satisfied. Otherwise, the values of $\xi_1$ and $\xi_2$ are rejected and a new pair is introduced.

The angle of entry is randomly given in terms of the three direction cosines $\alpha$, $\beta$, $\gamma$ with respect to the $x$, $y$, $z$ axes where the first $\gamma$, i.e. $\gamma_0$, must be positive due to the assumption that molecules flow from the left to the right. If it is assumed that

$$\alpha = \sin\phi\cos\theta \tag{C.0.23a}$$

$$\beta = \sin\phi\sin\theta \tag{C.0.23b}$$

$$\gamma = \cos\phi \tag{C.0.23c}$$

we can generate three random numbers $\xi_1$, $\xi_2$, $\xi_3$ and form $\nu_1 = \xi_1$, $\nu_2 = \xi_2$, $\nu_3 = 2\xi_3 - 1$ in which $\nu_2^2 + \nu_3^2 \leq 1$ must be satisfied, otherwise we must pick another pair of $\xi_2$ and $\xi_3$. Then,

$$\alpha = (1 - \nu_1)^{1/2} \left[\frac{\nu_2^2 - \nu_3^2}{\nu_2^2 + \nu_3^2}\right] \tag{C.0.24}$$

$$\beta = (1 - \nu_1)^{1/2} \left[\frac{2\nu_2\nu_3}{\nu_2^2 + \nu_3^2}\right] \tag{C.0.25}$$

$$\gamma = \nu_1^{1/2} \tag{C.0.26}$$

After the first flight of length $S$, it moves to

$$x = x_0 + \alpha S \tag{C.0.27a}$$

$$y = y_0 + \beta S \tag{C.0.27b}$$

$$z = z_0 + \gamma S \tag{C.0.27c}$$

For free-molecule flow, the flight either terminates at the wall ($x^2 + y^2 = 1$), or the molecule passes out the end of the tube ($z = z_0 + \gamma S = L$). To find which of two cases occurs, the distances to the wall and to the outlet surface are calculated and compared. The shorter distance determines which of the two cases has occurred. If the molecule has a collision with the wall, $x^2 + y^2 = 1$, the distance denoted by $S_1$ is determined by

$$S_1 = -\frac{Q}{P} + \sqrt{\left(\frac{Q}{P}\right)^2 - \frac{R}{P}} \tag{C.0.28}$$

where

$$Q = \alpha^2 + \beta^2$$

$$P = \alpha x_0 + \beta y_0$$

$$R = x_0^2 + y_0^2 - 1$$

If the molecule goes out the tube at $z = L$, the corresponding distance denoted by $S_2$ is given by

$$S_2 = \frac{L - z_0}{\gamma} = \frac{L}{\gamma} \tag{C.0.29}$$

Thus, for $S_1 \leq S_2$, a wall collision with the cylinder occurs and the distance to the collision is

$$S = S_1 \tag{C.0.30}$$

Or, $S_2 < S_1$, the molecule leaves the cylinder at the outlet $z = L$.

If the molecule has a collision with the wall, the new coordinates of the collision point are determined. There are

$$x = x_0 + \alpha S_1 \tag{C.0.31a}$$

$$y = y_0 + \beta S_1 \tag{C.0.31b}$$

$$z = z_0 + \gamma S_1 \tag{C.0.31c}$$

It is obvious that $x^2 + y^2 = 1$ at the new position.

When molecules collide with the wall of the cylinder, it is assumed that molecules are diffusely reflected, i.e., there is no preferential direction of reflection and the the scattering angle (i.e. the angle between the normal to the surface and the direction of the scattered molecule) is distributed as the cosine. Therefore, the new flight direction cosines at the new position $(x, y, z)$ are given by (see Appendix D in details)

$$\alpha' = \frac{\beta y - \gamma x}{\sqrt{x^2 + y^2}} \tag{C.0.32a}$$

$$\beta' = \frac{-\beta x - \gamma y}{\sqrt{x^2 + y^2}} \tag{C.0.32b}$$

$$\gamma' = -\alpha \tag{C.0.32c}$$

where $(\alpha, \beta, \gamma)$ is the scattering direction cosines which are randomly generated in the same way as Eqs.(C.0.24) - (C.0.26).

With the new position $(x, y, z)$ and flight direction cosines $(\alpha', \beta', \gamma')$, the next calculation is to determine whether the molecule has another collision with the wall, passes through the tube at $z = L$, or returns to the inlet surface at $z = 0$. This decision is made by comparing the distances $S_0$, $S_1$and $S_2$ as before.

The flight distance $S_1$ for a collision with the wall, i.e., $(x + \alpha' S_1)^2 + (y + \beta' S_1)^2 = 1$, solving it gives

$$S_1 = -\frac{2\left(\alpha'^2 + \beta'^2\right)}{\alpha' x + \beta' y} \tag{C.0.33}$$

The flight distance $S_0$ for leaving the tube at the inlet surface $z = 0$, i.e., $z + \gamma' S_0 = 0$,

$$S_0 = -\frac{z}{\gamma'} \tag{C.0.34}$$

The flight distance $S_2$ for leaving the tube at the outlet surface $z = L$, i.e., $z + \gamma' S_2 = L$,

$$S_2 = \frac{L - z}{\gamma'} \tag{C.0.35}$$

If $S_1$ is the shortest distance, the new position coordinates are calculated by Eqs.(C.0.31a) - (C.0.31c). The molecule will continue its flight within the tube and the above steps will be repeated until the molecule leaves the tube. If $S_0$ or $S_2$ is the least, the

simulation of the molecule flight at this time is terminated. But the number of molecules passing through the tube denoted by $N_{\mathrm{out}}$ is counted when $S_2$ is the least. Finally, the TP $\eta$ can be evaluated by the definition as $\eta = N_{\mathrm{out}}/N_{\mathrm{in}}$, in which $N_{\mathrm{in}}$ is the total number of molecules during the simulation.

# Appendix D

# Direction Cosines of the Diffusive Reflection

1. Unit normal direction of a given surface

Assuming a surface $S$ is given implicitly, i.e., the set of points ($x$, $y$, $z$) satisfying $F(x, y, z) = 0$. Thus, a normal direction (upward to the surface) at a point $P(x, y, z)$ on the surface is given by the gradient

$$\nabla F(x, y, z) = \frac{\partial F}{\partial x}\widehat{i} + \frac{\partial F}{\partial y}\widehat{j} + \frac{\partial F}{\partial z}\widehat{k} \tag{D.0.36}$$

The unit normal direction $\boldsymbol{\mu} = (\mu_x, \mu_y, \mu_z)$ at point $P\,(x, y, z)$is thus written as

$$\mu_x = \frac{\dfrac{\partial F}{\partial x}\,|_P}{A} \tag{D.0.37a}$$

$$\mu_y = \frac{\dfrac{\partial F}{\partial y}\,|_P}{A} \tag{D.0.37b}$$

$$\mu_z = \frac{\dfrac{\partial F}{\partial z}\,|_P}{A} \tag{D.0.37c}$$

where

$$A = |\nabla F\,(x, y, z)| = \sqrt{\left(\frac{\partial F}{\partial x}\right)^2 + \left(\frac{\partial F}{\partial y}\right)^2 + \left(\frac{\partial F}{\partial z}\right)^2} \tag{D.0.38}$$

2. New direction cosines with respect to a scattering angle $(\Theta, \Phi)$

Given an initial direction defined by $(\theta, \phi)$ and the scattering angles $(\Theta, \Phi)$ with respect to the initial condition where $\theta$, $\Theta$ are polar angles, and $\phi$, $\Phi$ are azimuthal angles. The initial and new direction cosines are denoted by $\boldsymbol{\mu} = (\mu_x, \mu_y, \mu_z)$ and $\boldsymbol{\mu'} = \left(\mu'_x, \mu'_y, \mu'_z\right)$, respectively. Thus

$$\mu_x = \sin\theta\cos\phi \tag{D.0.39a}$$

$$\mu_y = \sin\theta\sin\phi \tag{D.0.39b}$$

$$\mu_z = \cos\theta \tag{D.0.39c}$$

The new direction cosines $\boldsymbol{\mu'}$ can be determined from the initial direction, the polar scattering angle $\Theta$ and the azimuthal scattering angle $\Phi$ as

$$\begin{bmatrix} \mu'_x \\ \mu'_y \\ \mu'_z \end{bmatrix} = \begin{bmatrix} \dfrac{\mu_x\mu_z}{\sqrt{1-\mu_z^2}} & \dfrac{-\mu_y}{\sqrt{1-\mu_z^2}} & \mu_x \\ \dfrac{\mu_y\mu_z}{\sqrt{1-\mu_z^2}} & \dfrac{\mu_x}{\sqrt{1-\mu_z^2}} & \mu_y \\ -\sqrt{1-\mu_z^2} & 0 & \mu_z \end{bmatrix} \begin{bmatrix} \sin\Theta\cos\Phi \\ \sin\Theta\sin\Phi \\ \cos\Theta \end{bmatrix} \tag{D.0.40}$$

3. Direction cosines of diffusive reflection

It is assumed that the walls of the container are "molecularly rough", which implies that molecules striking the walls are reflected according to the cosine law and the reflection direction is independent of the incident direction. Thus, the new flight direction is random after the molecule collides with the wall at the point $P\,(x, y, z)$. This phenomena can also be described that the normal direction cosine $\boldsymbol{\mu} = (\mu_x, \mu_y, \mu_z)$ at point $P\,(x, y, z)$, but the scattering angle $(\Theta, \Phi)$ is random with the condition $0 \leq \Theta \leq \pi/2$ . Mathematically, the new flight direction can be expressed by Eq.(D.0.40).

Take a straight cylindrical tube as an example. The surface of a cylinder is described by

$$F\,(x, y, z) = x^2 + y^2 - 1 = 0 \tag{D.0.41}$$

In terms of Eqs.(D.0.36) - (D.0.38), the unit normal direction (downward to the surface) is calculated by

$$\mu_x = -\frac{x}{\sqrt{x^2+y^2}} \tag{D.0.42a}$$

$$\mu_y = -\frac{y}{\sqrt{x^2+y^2}} \tag{D.0.42b}$$

$$\mu_z = 0 \tag{D.0.42c}$$

Thus, the new flight direction of the molecule after collision with the wall can be determined by

$$\begin{bmatrix} \mu_x' \\ \mu_y' \\ \mu_z' \end{bmatrix} = \begin{bmatrix} 0 & \frac{y}{\sqrt{x^2+y^2}} & -\frac{x}{\sqrt{x^2+y^2}} \\ 0 & -\frac{x}{\sqrt{x^2+y^2}} & -\frac{y}{\sqrt{x^2+y^2}} \\ -1 & 0 & 0 \end{bmatrix} \begin{bmatrix} \sin\Theta\cos\Phi \\ \sin\Theta\sin\Phi \\ \cos\Theta \end{bmatrix} \tag{D.0.43}$$

or

$$\mu_x' = \frac{y}{\sqrt{x^2+y^2}}\beta - \frac{x}{\sqrt{x^2+y^2}}\gamma \tag{D.0.44a}$$

$$\mu_y' = -\frac{x}{\sqrt{x^2+y^2}}\beta - \frac{y}{\sqrt{x^2+y^2}}\gamma \tag{D.0.44b}$$

$$\mu_z' = -\alpha \tag{D.0.44c}$$

where

$$\alpha = \sin\Theta\cos\Phi \tag{D.0.45a}$$

$$\beta = \sin\Theta\sin\Phi \tag{D.0.45b}$$

$$\gamma = \cos\Theta \tag{D.0.45c}$$

During the calculation, $(\alpha, \beta, \gamma)$ can be randomly generated to simulate the diffusive reflection after the molecule has a collision with the wall.

# Appendix E

# Probability Functions of the Diverging-Converging Tube

Mathematical expressions of probabilities from ring or section to (another) ring or section, $\omega$'s, in the conically diverging-converging tube are calculated as follows

**1. From section to section** $\omega_{ss}$

$$\omega_{ss}(L) = 1 - \frac{2L}{L + \sqrt{L^2 + 4r_0^2}} \tag{E.0.46}$$

**2. From section to ring** $\omega_{sr}$

(a) $0 \leq z \leq \dfrac{L}{2}$

$$\omega_{sr}(z) = \frac{1}{r_0^2}\left[\frac{\sec\beta\left(z^2\sec^2\beta + 3r_0 z\tan\beta + 2r_0^2\right)}{\sqrt{z^2\sec^2\beta + 4r_0 z\tan\beta + 4r_0^2}} - \left(z\sec^2\beta + r_0\tan\beta\right)\right] \tag{E.0.47a}$$

(b) $\dfrac{L}{2} \leq z \leq L$

$$\omega_{sr}(z) = \frac{1}{r_0^2}\left[\frac{z\left(r_2^2 + z^2 + r_0^2\right) - r_2\tan\beta\left(r_2^2 + z^2 - r_0^2\right)}{\sqrt{\left(r_2^2 + z^2 + r_0^2\right)^2 - 4r_0^2 r_2^2}} - \left(z + r_2\tan\beta\right)\right] \tag{E.0.47b}$$

**3. From ring to section** $\omega_{rs}$

(a) $0 \le z \le \dfrac{L}{2}$

$$\omega_{rs}(L-z) = \frac{\cos\beta}{2r_2}\left[\frac{(L-z)\left(r_2^2+(L-z)^2+r_0^2\right)-r_2\tan\beta\left(r_2^2+(L-z)^2-r_0^2\right)}{\sqrt{\left(r_2^2+(L-z)^2+r_0^2\right)^2-4r_0^2r_2^2}} - \left((L-z)-r_2\tan\beta\right)\right] \tag{E.0.48a}$$

(b) $\dfrac{L}{2} \le z \le L$

$$\omega_{rs}(L-z) = \frac{\cos\beta}{2r_2}\left[\frac{\sec\beta\left((L-z)^2\sec^2\beta+3r_0(L-z)\tan\beta+2r_0^2\right)}{\sqrt{(L-z)\sec^2\beta+4r_0(L-z)\tan\beta+4r_0^2}} - \left((L-z)\sec^2\beta+r_0\tan\beta\right)\right] \tag{E.0.48b}$$

**4. From ring to ring** $\omega_{rr}$

(a) $0 \le y, z \le \frac{1}{2}L$ or $\frac{1}{2}L < y, z \le L$

$$\omega_{rr}(y-z) = \frac{\cos\beta}{2r_z}\left[1-\frac{|y-z|\sec\beta\left((y-z)^2\sec^2\beta+6r_zr_y\right)}{\sqrt{\left((y-z)^2\sec^2\beta+4r_zr_y\right)}}\right] \tag{E.0.49a}$$

where

$$r_z = \begin{cases} r_0+\dfrac{2\alpha r_0}{L}z, & 0 \le z \le \dfrac{L}{2} \\ r_0+\dfrac{2\alpha r_0}{L}(L-z), & \dfrac{L}{2} < z \le L \end{cases}$$

$$r_y = \begin{cases} r_0+\dfrac{2\alpha r_0}{L}y, & 0 \le x \le \dfrac{L}{2} \\ r_0+\dfrac{2\alpha r_0}{L}(L-y), & \dfrac{L}{2} < y \le L \end{cases}$$

(b) $0 \leq y \leq \frac{1}{2}L < z < L$ or $0 \leq z \leq \frac{1}{2}L < y < L$

$$\begin{aligned} \omega_{rr}(y-z) &= 2r_y \cos\beta \left[ \frac{b_0 d_0}{f_0^2} \left( 1 - \frac{e_0}{\sqrt{e_0^2 - f_0^2}} \right) \right. \\ &\quad \left. + \frac{e_0(a_0 c_0 + b_0 d_0) - f_0(a_0 d_0 + b_0 c_0)}{(e_0^2 - f_0^2)^{3/2}} \right] \end{aligned} \tag{E.0.49b}$$

where $a_0 = r_z + |y-z| \tan\beta$, $b_0 = r_y$, $c_0 = r_y + |y-z| \tan\beta$, $d_0 = r_z$, $e_0 = x^2 + r_z^2 + r_y^2$, and $f_0 = 2r_z r_y$.

# Appendix F

# Probability Functions of the Bulging Tube

Mathematical expressions of probabilities from ring or section to (another) ring or section, $\omega$'s, in the bulging (sinusoidally diverging-converging) tube are calculated as follows

**1.** $\omega_{ss}(z)$ **is identical**

**2.** $\omega_{sr}(z)$

(a) $0 < z < L$

$$\omega_{sr}(z) = \frac{1}{r_0^2}\left[\frac{z\left(r^2+z^2+r_0^2\right) - r\tan\beta\left(r^2+z^2-r_0^2\right)}{\sqrt{\left(r^2+z^2+r_0^2\right)^2 - 4r_0^2r^2}} - \left(z + r\tan\beta\right)\right] \tag{F.0.50a}$$

where $\tan\beta = \dfrac{\alpha r_0 \pi}{L}\cos\dfrac{\pi z}{L}$.

(b) $z = 0$

$$\omega_{sr}(0) = \frac{1}{r_0}\left\{\left[1+\left(\frac{\pi\alpha r_0}{L}\right)^2\right]^{1/2} - \frac{\pi\alpha r_0}{L}\right\} \tag{F.0.50b}$$

**3.** $\omega_{rs}(L-z)$

(a) $0 < z < L$

$$\omega_{rs}(L-z) = \frac{\cos\beta}{2r}\left[\frac{(L-z)\left(r^2+(L-z)^2+r_0^2\right)-r\tan\beta\left(r^2+(L-z)^2-r_0^2\right)}{\sqrt{\left(r^2+(L-z)^2+r_0^2\right)^2-4r_0^2r^2}} - \left((L-z)-r\tan\beta\right)\right] \tag{F.0.51a}$$

(b) $z = L$

$$\omega_{sr}(0) = \frac{\cos\beta}{2}\left\{\left[1+\left(\frac{\pi\alpha r_0}{L}\right)^2\right]^{1/2} - \frac{\pi\alpha r_0}{L}\right\} \tag{F.0.51b}$$

**4.** $\omega_{rr}(y-z)$

(a) $z \neq y$

$$\omega_{rr}(y-z) = 2r_y\cos\beta_z\left[\frac{b_0d_0}{f_0^2}\left(1-\frac{e_0}{\sqrt{e_0^2-f_0^2}}\right) + \frac{e_0(a_0c_0+b_0d_0)-f_0(a_0d_0+b_0c_0)}{\left(e_0^2-f_0^2\right)^{3/2}}\right] \tag{F.0.52a}$$

where $a_0 = r_z + |y-z|\tan\beta_z$, $b_0 = r_y$, $c_0 = r_y + |y-z|\tan\beta_y$, $d_0 = r_z$, $e_0 = x^2 + r_z^2 + r_y^2$, $f_0 = 2r_zr_y$, $r_z = a + \alpha a\sin\dfrac{\pi z}{L}$, $\tan\beta_z = \dfrac{\pi\alpha a}{L}\cos\dfrac{\pi z}{L}$, $r_y = a + \alpha a\sin\dfrac{\pi y}{L}$, and $\tan\beta_y = \dfrac{\pi\alpha a}{L}\cos\dfrac{\pi y}{L}$.

(b) $z = y$

$$\omega_{rr}(0) = \frac{\cos\beta_z}{2r_z} \tag{F.0.52b}$$

# Bibliography


[1] Suresh Bhatia and David Nicholson. Some pitfalls in the use of the knudsen equation in modelling diffusion in nanoporous materials. *Chemical Engineering Science*, 66(3):284–293, Feb 2011.

[2] Suresh K Bhatia, Owen Jepps, and David Nicholson. Tractable molecular theory of transport of lennard-jones fluids in nanopores. *J. Chem. Phys.*, 120(9):4472, Jan 2004.

[3] Vincenza Calabro, Bi Jiao, and Enrico Drioli. Theoretical and experimental study on membrane distillation in the concentration of orange juice. *Ind. Eng. Chem. Res.*, 33(7):1803–1808, Jul 1994. doi: 10.1021/ie00031a020.

[4] P Clausing. Uber die stromung sehr verdunnter gase durch rohren von beliebiger lange. *Ann. Phys. (Leipzig)*, 12:961–989, Oct 1932.

[5] P Clausing. The flow of highly rarefied gases through tubes of arbitrary length. *The Journal of Vacuum Science and Technology*, 8(5):636–756, Apr 1971.

[6] D H Davis. Monte carlo calculation of molecular flow rates through a cylindrical elbow and pipes of other shapes. *J. Appl. Phys.*, 31(7):1169–1176, Jul 1960.

[7] N Diban, O Voinea, A Urtiaga, and I Ortiz. Vacuum membrane distillation of the main pear aroma compound: Experimental study and mass transfer modeling. *J. Membr. Sci.*, 326(1):64–75, Jan 2009.

[8] C. A Flory and L. S Cutler. Integral equation solution of low-pressure transport of gases in capillary tubes. *J. Appl. Phys.*, 73(4):1561, Jan 1993.

[9] Raymond P Iczkowski, Raymond P Iczkowski, John L Margrave, John L Margrave, Stephen M Robinson, and Stephen M Robinson. Effusion of gases through conical orifices. *J. Phys. Chem.*, 67(2):229–233, 1963.

[10] R Evans III, G Watson, and E Mason. Gaseous diffusion in porous media at uniform pressure. *J. Chem. Phys.*, 35(6):2076–2083, Dec 1961.

[11] R Evans III, G Watson, and E Mason. Gaseous diffusion in porous media. ii. effect of pressure gradients. *J. Chem. Phys.*, 36(7):1894–1902, Apr 1962.

[12] Martin Knudsen. Die gesetze der molekularströmung und der inneren reibungsströmung der gase durch röhren. *Ann. d. Physik*, 333(1):75–130, 1909.

[13] Martin Knudsen and Willard Fisher. The molecular and the frictional flow of gases in tubes. *Phys. Rev. (Series I)*, 31(5):586, Nov 1910.

[14] A Kogan. Direct solar thermal splitting of water and on-site separation of the products–ii. experimental feasibility study. *International Journal of Hydrogen Energy*, 23(2):89–98, 1998.

[15] Rajamani Krishna and Jasper M van Baten. A molecular dynamics investigation of the unusual concentration dependencies of fick diffusivities in silica mesopores. *Microporous and mesoporous materials*, 138(1-3):228–234, 2011.

[16] Young-Il Lim and Suresh Bhatia. Simulation of methane permeability in carbon slit pores. *Journal of Membrane Science*, 369(1-2):319–328, Mar 2011.

[17] P J Lobo, Fulvio Becheri, and J Gomez-Goni. Comparison between monte carlo and analytical calculation of clausing functions of cylindrical and conical tubes. *Vacuum*, 76:83–88, 2004.

[18] E Mason, A Malinauskas, and R Evans III. Flow and diffusion of gases in porous media. *J. Chem. Phys.*, 46(8):3199–3216, Apr 1967.

[19] W G Pollard and R D Present. On gaseous self-diffusion in long capillary tubes. *Phys. Rev.*, 73(7):762 – 774, 1948.

[20] R. D Present and A J DeBethune. Separation of a gas mixture flowing through a long tube at low pressure. *Phys. Rev.*, 75(7):1050–1057, Apr 1949.

[21] Frederick Reif. *Fundamentals of Statistical and Thermal Physics*. McGraw-Hill, New York, 1965.

[22] Thaine W Reynolds and Edward A Richley. Flux patterns resulting from free-molecule flow through converging and diverging slots. *NASA Tech. Note*, TN D-1864:1–69, 1964.

[23] Thaine W Reynolds and Edward A Richley. Free molecule flow and surface diffusion through slots and tubes - a summary. *NASA Technical Report*, TR R-255, 1967.

[24] Edward A Richley and Thaine W Reynolds. Numerical solutions of free-molecule flow in converging and diverging tubes and slots. *NASA Tech. Note*, TN D-2330:1–45, Nov 1964.

[25] Douglas M Ruthven, W J Desisto, and S Higgins. Diffusion in a mesoporous silica membrane: Validity of the knudsen diffusion model. *Chem. Eng. Sci.*, 64:3201 — 3203, May 2009.

[26] W Steckelmacher. Knudsen flow 75 years on: the current state of the art for flow of rarefied gases in tubes and systems. *Rep. Prog. Phys.*, 49:1083–1107, Jan 1986.

[27] Wilson K Talley and Stephen Whitaker. Monte carlo analysis of knudsen flow. *J. Comp. Phys.*, 4(3):389–410, Oct 1969.

[28] Stelio Villani. *Isotope Separation*. American Nuclear Society, 1976.

[29] John W T Walsh. Radiation from a perfectly diffusing circular disc (part i). *Proceedings of the Physical Society of London*, 32:59, Dec 1919.